

DOI: 10.1002/ ((please add manuscript number))

Article type: (Review)

Organic Flexible Electronics

*Haifeng Ling, Shenghua Liu, Zijian Zheng and Feng Yan**

Dr. H.F. Ling, Dr. S.H. Liu, Prof. F. Yan
Department of Applied Physics, The Hong Kong Polytechnic University,
Hong Kong, China
E-mail: apafyan@polyu.edu.hk

Prof. Z. J. Zheng
Institute of Textiles Clothing,
The Hong Kong Polytechnic University,
Hung Hom, Kowloon, Hong Kong.

Keywords: Organic Electronics, Flexible, OLEDs, OPVs, OTFTs

Abstract. During the past two decades, the vigorous development of flexible organic semiconductor devices has heralded a new era of human society due to their promising applications in portable, wearable, implantable and biological electronics. In recent years, exciting progress has been made on various flexible electronic devices, including organic light-emitting diodes, organic photovoltaics, organic thin-film transistors, organic flexible integrated circuits, sensors and memories. To provide a comprehensive and up-to-date review on this emerging field, we focus on critical issues of organic devices, including material choice, device design, mechanical flexibility, strain effects and processing techniques, as well as some specific applications that have been successfully developed. Finally, we give a conclusion and outlook for the future development of this field.

1. Introduction

Since the 1960s, the silicon-based semiconductor industry has been a cornerstone of modern information society. Traditional complementary metal–oxide–semiconductor (CMOS) systems are rigid integrations composed of stiff circuit boards and hard silicon-based chips and are unable to meet a demand of flexibility for the upcoming era of wearable electronics, robotics and artificial intelligence.^[1-3] The term “flexible electronics” refers to the class of thin-film electronic devices that can be bent, folded, twisted, compressed, stretched, and even deformed into arbitrary shapes but still maintain a high electrical performance, reliability, and integration. The discovery of highly conducting polyacetylene by Shirakawa, MacDiarmid, and Heeger in 1977 birthed a new exciting world of organic electronics based on π -conjugated systems.^[4] Combined with the intrinsic light weight, softness and tunable device performance *via* molecular tailoring, organic flexible electronics have received much attention from both the academic and industrial communities.^[5] Owing to the key features of low cost and low-temperature processability over arbitrary substrates, solution-processed organic semiconductors (OSCs) are amenable to inexpensive and high-throughput manufacturing to fulfill the constantly increasing demand for large-area electronics.^[6, 7] Furthermore, some specific OSCs possessing favorable properties of biocompatibility or biodegradability,^[8, 9] enable organic flexible electronic arrays to seamlessly interface with biological systems, leading to numerous human-friendly applications, such as electronic skins and smart prosthetics,^[10] wearable human-activity/health monitoring devices.^[11]

A major issue of concern for organic flexible electronics is often a trade-off existing between the best electronic properties and device flexibility. To develop high-performance organic flexible devices, various approaches have been reported, mainly focusing on the following four aspects (**Figure 1**): i) intrinsically flexible organic components (semiconductor, electrode, insulator, and substrate), ii) structural engineering, iii) fundamental mechanical

deformability and iv) continuous processing technique. Each part will be discussed in detail in the following sections.

First, with their intrinsically low elastic modulus (especially the Young's modulus),^[5] organic materials are naturally pliable to increased strain in fully flexible devices. The emergence of organic conjugated semiconductors based on small molecules and polymers has enabled the development of active layers for various flexible organic electronics.^[12] Nano-materials (3D, 2D, 1D, 0D),^[13, 14] biological materials,^[15, 16] ferroelectric polymers,^[17] and thermoelectric materials^[18] are also promising candidate materials for the preparation of flexible electronics. In addition to conventional thick and brittle conductive electrodes (e.g., Au, Cu, Ag, and ITO), novel technologies such as semitransparent metallic mesh electrodes,^[19, 20] poly(3,4-ethylenedioxythiophene):poly(styrenesulfonate) (PEDOT:PSS)-based electrodes,^[21-23] paper-based electrodes,^[24] graphene electrodes,^[25] polymer composites with conducting fillers^[26-28] exhibit high transparency, conductivity, mechanical compliancy and empower functionalities such as self-healing.^[29, 30] These electrode materials are particularly suitable for fabrication on a wide variety of soft substrates, including plastics (e.g., polyethyleneterephthalate (PET), polyethylene-2, 6-naphthalate (PEN), parylene), elastomers (e.g., poly(dimethylsiloxane) (PDMS), polyimide (PI)), papers, and fiber (textiles).^[31] Additionally, stability and lifetime of flexible devices under ambient or even harsh conditions are critical to commercialization. Most organic semiconducting materials are vulnerable to some conditions such as the exposure to water, oxygen, heat, chemicals, and light irradiation.^[32] In addition to the optimization of molecular design and materials syntheses, an efficient approach used thus far has been the adoption of an encapsulation layer to protect the final devices from extrinsic degradation sources. For this purpose, PDMS,^[33, 34] PI,^[35] Parylene C^[36] and CYTOP^[37] are commonly used organic encapsulation materials in flexible electronics, without affecting device flexibility.

Second, structural engineering is an indispensable strategy to improve deformation tolerance by introducing flexible interconnects (e.g., arc-shaped, serpentine, or mesh-shaped interconnects)^[38] and pre-strained elastomeric patterns (e.g., waved, buckled, wrinkled, square-shaped, pyramid-shaped, microcracked or porous patterns).^[39] The two strategies are complementary and mainly focus on the configuration design of flexible electrodes and substrates.^[40] Then, the flexible materials or devices are directly transferred or printed on these flexible templates to absorb a larger level of strain than the intrinsic critical strain of the films. The above engineering technique is especially useful to impart stretchability to non-stretchable but flexible components. Other strategies are to place the active layer in the neutral strain position,^[34] or to reduce the total thickness of the devices to a few microns, both of which are suitable for bendable and foldable devices to further suppress the strain.^[41] Besides ingenious device design or precise morphology control, structural engineering could potentially provide an additional boost to deformation tolerance as well as device lifetime.^[42, 43]

Third, internal electrical stability under external mechanical stimulation is fundamental to organic flexible electronics. Important mechanical properties include stiffness, strength, toughness, damping, and fatigue resistance. For advanced applications, transparency,^[44] biodegradability,^[16] self-healing^[45] and self-powering^[46] are also considered. The testing and assessment of flexible devices include mechanical deformability under both static and dynamic conditions. Static mode consists of bending, rolling (folding), twisting (crumpling) and stretching, while dynamic mode refers to repeated/cycled mechanical stimulation. The critical strain (ϵ_{crit}) is defined as the radius of curvature at which device failure occurs because of mechanical damage or functional failure (e.g., electrical failure). Depending on the critical strain level, the flexibility can be divided into three categories: flexible electronics ($\epsilon_{\text{crit}} < 2\%$, e.g., bending), compliant electronics ($2\% < \epsilon_{\text{crit}} < 10\%$, e.g., folding, rolling or twisting) and stretchable electronics ($\epsilon_{\text{crit}} > 10\%$).^[47] A low Young's (or tensile) modulus is highly desirable

for the above deformable applications, which is closely related to molecular structure. Generally, brittle deformation beyond a typically low ϵ_{crit} results in total failure. Tough materials also show irreversible deformation beyond a much higher ϵ_{crit} . Therefore, elastomeric deformation is required for flexible electronics, which is characterized by reversible strain of several hundred percent.^[48]

Fourth, a continuous processing technology is among the key issues for flexible electronics. Currently, spin-casting can only deposit uniform thin films suitable for small-area devices (laboratory-scale, typically $\sim 1 \text{ cm}^2$). Despite vacuum-thermal evaporation is already used commercially in the fabrication of organic light-emitting diode (OLED) displays, vacuum-compatible roll-to-roll (R2R) approach to produce high-speed, low-cost and large-area organic electronic circuits is still open to challenge.^[49] To this end, two solution-processing approaches, namely, coating and printing, have been employed, and both have good compatibility with low-temperature, large-volume and high-throughput R2R production of organic flexible electronics. Coating techniques are generally noncontact and one-dimensional techniques, thereby, an important source of particle contamination and other damage to the device is eliminated. Typical coating approaches include doctor-blade (or bar) coating,^[50-52] slot die coating,^[53, 54] and spray coating.^[55, 56] Well-known printing methods include inkjet, screen, and gravure printing.^[57] Novel 3D-printing technology is also now being applied to fabricate flexible electronics with complicated geometries.^[58] The important printing parameters are resolution, accuracy, uniformity over a large area, compatibility of inks with printing components, wettability of target substrate, throughput.^[6] Solution-based functional inks, such as conjugated molecules, sol-gel-processed metal oxide precursors, and nanocarbon-based materials, enable the realization of thin-film electronics using graphic art printing processes. By manufacturing through a combination of various coating and printing methods, R2R technology delivers superior compatibility with future flexible electronics.^[59] It is important to note the reliability of R2R organic circuit production, with a particular focus

on chemical stability of organic materials related to fabrication processes. For example, the use of vaporized organic solvents or acidic/basic solutions increases the possibility for the contamination of organic components, which might result in variation in material quality and device performance. The solvent resistance of organic semiconductors can be enhanced through crosslinking or side-chain engineering.^[60, 61] Solvent-free method *via* initiated chemical vapor deposition (iCVD) is also a high-volume commercial process, and has shown great potentialities for R2R producing of robust organic conductors and insulators.^[62, 63]

The aim of this review is to provide a wide and up-to-date overview on the fast-growing research field of organic flexible electronics. We will elaborate on important developments in emerging flexible electronic/optoelectronic devices, such as OLEDs, organic photovoltaics (OPVs), organic thin film transistor (OTFT)-based flexible organic circuits, biological/physical sensors and memories. In particular, integrated platforms combining the aforementioned flexible electronics for future biocompatible and implanted electronic devices are introduced to exemplify their potential. Conclusions and prospects are discussed at the end to provide a guideline for future research.

2. Flexible OLEDs

OLEDs represent the first commercial success for organic electronics. Flexible OLEDs are remarkably promising devices for future display and solid-state lighting technology, as they can function in mechanically flexible configurations on a plastic substrate due to their various compelling properties, including organic constituents, ultrathin and simple structure, and low-temperature fabrication.^[64]

2.1. Materials

An OLED is a light-emitting diode in which the electroluminescent emitter is an organic material that emits light in response to a driving current. Based on the difference in emitters, OLEDs are usually categorized into fluorescent OLEDs, phosphorescent OLEDs and

thermally activated delayed fluorescence (TADF) OLEDs.^[65, 66] The first-generation OLEDs were based on small-molecule fluorescent emitters, such as 4-(dicyanomethylene)-2-methyl-6-[p-(dimethylamino) styryl]-4H-pyran (DCM) derivatives (red), rubrene (red), coumarin 6 (green), quinacridone (green), Alq₃ (green), anthracene derivatives (blue), fluorene derivatives (blue), and distyrylarylene (blue).^[67] Despite their significant advantages in device performance, such as current efficiency (CE), external quantum efficiency (EQE) and operating lifetime, fluorescent OLEDs mainly suffer from low exciton utility in which only 25% of total excitons can generate light, resulting in a limited EQE (generally <5%).^[68] To harvest both singlet and triplet excitons, heavy metal atoms such as Cu, Ir, Pt, are introduced into molecular structure to enhance spin-orbital coupling, and promote intersystem crossing and emit phosphorescence efficiently.^[69] An alternative strategy to utilize triplet excitons is TADF,^[70, 71] which has a small difference between singlet and triplet states, and triplet excitons could efficiently change back to singlet excitons. Both PhOLED and TADF OLED can realize 100% internal quantum efficiency. Yet both types have high triplet exciton densities, exciton quenching is serious in devices, leading to obvious efficiency roll-off under high current densities. The doping of an emitter into a host matrix with higher triplet energy levels (e.g., carbazole and/or triphenylamine derivatives) has proved to be a successful strategy to achieve host–guest OLEDs with high emission efficiency.^[72, 73]

Small-molecule OLEDs (SMOLEDs) are now widely used in mobile device displays. As trends are shifting towards large-sized and/or flexible/wearable displays, polymer emissive materials-based OLEDs (PLEDs) have received much attention due to their intrinsic applicability with large-area R2R processing. Another noteworthy feature of polymer emissive materials is that the required functions (charge-carrier injection/transporting, emissive units, etc.) can be introduced into polymer chains by co-polymerization and the addition of functional units. In addition, polymer emitters show not only red, green, and blue (RGB) emission but also white emission.^[74] As a result, polymer-based OLEDs can function

well without a complex multilayer device structure. Generally, polymer emissive materials can be divided into two classes: conjugated polymers with a delocalized π -electron system and polymers with functional units attached to a non-conjugated backbone. For conjugated-polymer emitters, polyphenylenevinylene (PPV), polyfluorene (PF), and poly-p-phenylene (PPP) are typical examples that emit in the visible region.^[75, 76] In addition, π -stacked poly(vinylcarbazole) (PVK) is a typical non-conjugated polymer with a relatively high triplet energy state along with excellent hole-transporting ability, which is also used extensively as a host material.^[77] On the other hand, the design of π -stacked polymers opens another avenue to the development of polymer hosts for red, green, and blue emitters. However, polymers may have issues concerning their molecular weight, polydispersity index (PDI), and distribution of different monomers in their backbones. All these factors influence their electroluminescent (EL) performance. Besides, polymer based OLEDs are more limited by current efficiency, lifetime and stability problems than their small-molecule counterparts.^[78]

For display and lighting applications, one of the electrodes is required to be transparent to allow the produced light to escape, and indium tin oxide (ITO, 5~10 Ω /sq at small area), which possesses a high work function, is the most popular anode material. The cathode material is usually a metal with a lower work function, such as Ag, Al, Mg, or Ca. From the standpoint of flexible OLEDs, one of the technical challenges is to find a highly conductive and transparent electrode material that can also withstand large strains. Poly(3,4-ethylenedioxythiophene):poly(styrenesulfonate) (PEDOT:PSS),^[79] carbon based materials (e.g., carbon nanotubes (CNTs), graphene^[80]) and metallic networks (e.g., silver nanowires (Ag NWs)^[81]) show remarkable advantages of high transparency, conductivity, mechanical compliance, and solution processability.^[27] Among them, Ag NWs have similar optoelectronic performances to ITO and are potential candidates to replace ITO.^[82] However, Ag NWs directly coating on substrates have large surface height variations greater than 100 nm, resulting in poor performance of the OLEDs.^[51] One current alternative is to employ a Ag

NW-polymer composite, such as Ag NW-polyvinyl alcohol (PVA),^[81] Ag NW-PMMA,^[83] Ag NW-polyimide (PI),^[84] Ag NW-colorless polyimide (cPI),^[43] or Ag NW-poly(urethane acrylate) (PUA).^[85] This approach usually creates a two-in-one electrode and substrate with intrinsically flexibility. For example, Pei and co-workers^[86] fabricated an Ag NW-poly(acrylate) electrode with a surface roughness less than 5 nm. The Ag NW films can be tailored to the desired transparency and conductivity by controlling the amount of solid nanowires. The transmittance at 550 nm reaches 91% when the sheet resistance is 100 Ω /sq, which is comparable to commercially available ITO electrodes coated on PET substrates. The Ag NW electrodes can be bent up to 16% compressive strain with negligible change in sheet resistance. In addition, the resistance change is fully recovered when the deformed electrode returns to its undeformed shape. Moreover, it has been demonstrated that the use of the Ag NW-polymer substrate had an additional benefit of extracting more light emitted from the emissive layer in comparison to devices built on ITO/glass.^[87, 88]

PET, PEN, PI and PDMS are favorable candidates for the development of flexible OLED substrates. However, the controlled and ordered elasticity of the substrate is normally necessary but difficult to achieve. To overcome this obstacle, techniques based on the structural engineering of the substrate have been demonstrated by adhering an ultrathin OLED/polymer film onto a pre-strained elastomeric substrate with ordered buckling.^[48, 89] As shown in **Figure 2a**, Sun et al.^[89] used femtosecond (fs) laser ablation to fabricate one-dimensional (1D) long-period gratings with programmable parameters on the surface of an elastomeric substrate. Then, the peeled-off OLED/polymer film was transferred and attached to the prestretched elastomeric substrate. After releasing the strain, the suspended OLED thus exhibited the same period as that of the 1D gratings (Figure 2b-f). At strain values between 0 and 40% (Figure 2g), luminance was degraded by about 25% over 6,000 repeated stretch-release cycles.

For thin polymeric flexible substrates, a common shortcoming is that they suffer from permeability problems in moisture and oxygen environment due to the low density.^[90] Besides, when exposing the devices to ambient conditions, pre-existing defects (e.g., pin-holes) in the reactive cathode would lead to localized degradation, and generate diffusion pathways of moisture and oxygen, finally resulting in non-emissive areas (i.e., the dark spots).^[78] A flexible and high transparent encapsulation strategy to protect flexible OLEDs from the degradation of both the bottom and top sides is essential for commercial success.^[91] Currently, most OLEDs are encapsulated in glass incorporated with UV-cured epoxy and desiccant. Although it has excellent impermeability, rigid glass inhibits the possibility for flexible devices.^[92] Inorganic encapsulation materials, e.g., commercialized Al_2O_3 , SiO_x and SiN_x , show superior protection from moisture. However, they suffer from both factors of poor flexibility and pinhole defects in the layer surface.^[93] At present, inorganic/organic hybrid has been considered as one of the most effective barrier technologies of flexible OLEDs. Typical examples include ZnO/Parylene C,^[36] SiN-acrylate-SiN,^[94] $\text{Al}_2\text{O}_3/\text{ZrO}_2/\text{alucone}$,^[93] ZTO/ORMOCER[®]/ZTO,^[95] and polymer/graphite nanocomposites^[96] etc. Specifically, a water vapor transmission rate (WVTR) of less than 10^{-6} g/m²/day and an oxygen transmission rate (OTR) as low as 10^{-5} cm³/m²/day should be achieved to develop sufficient barriers for OLEDs.^[97]

2.2. Device Fabrication and Performance

The vacuum deposition of small-molecule materials is already well-established in the manufacture of OLED displays. Outstanding device efficiency and lifetime can be easily achieved in vacuum evaporation processes, especially for white OLEDs consisting of two or more multiple layers of different materials.^[98] Despite commercial R2R systems are already available for evaporating thin metal films in the food packaging industry, uniformity of vacuum deposition becomes an important issue for processing large-area OLEDs. Kim et al.^[99] studied thin film uniformity of flexible OLEDs in a R2R thermal evaporation system.

They demonstrated that the uniformities of the thin film in the scan direction (SD) and in the cross-scan direction (CD) are both critical to ensure the uniformity of the entire thin film. The SD uniformity could be achieved by precise velocity control in a high vacuum environment. Cho et al.^[84] reported a R2R process for preparing an embedded AgNWs transparent electrode on a PI film. 15 cm × 30 cm sized flexible green OLEDs were then deposited directly on the embedded AgNWs electrodes by a R2R vacuum deposition process. The initial luminance (500 cd/m²) of this flexible OLEDs decreased by 6% after 2000 times of bending at the 7 mm radius. Roll-to-roll manufacturing of substrate and encapsulation of small-molecule OLEDs are investigated by Fahlteich et al.^[95] 10 cm × 10 cm flexible white OLEDs with three-layered permeation barrier stacks have reached a WVTR down to 5×10^{-5} g/m²day at ambient condition on both PET and PEN substrates. However, vacuum deposition-based R2R processing for cost-effective OLEDs with low energy consumption still remains a challenge. Solution-processed R2R production on flexible substrates has always been the final goal for commercialized available OLED product. A variety of R2R compatible film deposition methods, such as inkjet printing,^[100, 101] screen printing,^[102] blade coating,^[103] slot-die coating^[53] and spray coating,^[83] have been adopted for the mass-production of flexible OLEDs.

Flexible OLEDs technology has enabled various new features to be added to modern electronics (**Table 1**). Highly flexible OLEDs with strains tolerance over 10% can generate a display conformability laminated onto arbitrary shaped surface.^[104] The combination of ultrathin OLEDs and substrate engineering paves the way towards high stretchability and high efficiencies. White and co-workers^[48] fabricated ultrathin 2 μm PLEDs with 1.4 μm PET foil substrates and subsequently transferred the PLEDs to a pre-stretched adhesive elastomer (VHB). Together with the semiconducting polymer materials with relatively high critical strain, the devices can operate under extreme flexing conditions with radii under 10 μm and demonstrated cyclic tensile strains up to 100%. The ultrathin and highly stretchable red

PLEDs showed a luminance of 32.7 ± 23.8 cd/m² at 9 V, and EQE of $0.08 \pm 0.04\%$, which is sufficient for indoor RGB displays. Someya and co-workers^[105] used RGB conjugated polymeric emissive materials to demonstrate 3 μ m ultraflexible and conformable three-color PLEDs to realize both seven-segment analog displays and digital displays on human skin (**Figure 3a-c**). In combination with the ultrathin device thickness, the design of the active layer in the neutral strain position and the pre-stretched wrinkled structure, the PLEDs were mechanically flexible with a bending radius of 100 μ m and did not degrade after 1000 cycles with 60% stretching (**Figure 3d**). These ultraflexible PLEDs exhibited remarkable EQE and blue (6.2% and 1000 cd/m², $\lambda_{\text{peak}} = 460$ nm), green (13.9% and 4900 cd/m², $\lambda_{\text{peak}} = 517$ nm) and red (12.4% and 2100 cd/m², $\lambda_{\text{peak}} = 609$ nm) luminance at a current density of 10 mA/cm². By integrating the ultraflexible green and red PLEDs with an organic photodetector (OPD), they further fabricated a flexible and conformable reflective pulse oximeter to monitor blood oxygenation when wrapped around a finger (**Figure 3e**). Light was emitted from the PLEDs to the body, and the reflected light was detected by the OPD. The sensing mechanism depended on the difference in the absorptivity of oxygenated and deoxygenated haemoglobin at different wavelengths.^[106] As a result, they succeeded in measuring pulsating photoplethysmogram (PPG) signals with amplitudes of approximately 100 to 200 mV (**Figure 3f-g**).

Apart from the application of pulse oximeter,^[103, 105, 106] OLED technology can provide visual feedback and can be used as point-of-care immunobio sensors,^[107] muscle contraction sensor,^[108] and stimuli-responsive sensors.^[109-111] Park et al.^[110] reported a PLED-based *in-situ* sensing board for achieving a dynamic interactive display that simultaneously detects external stimuli and visualizes the stimulant object. The board adopted an inverted OLED architecture that consisted of a Super Yellow/ multi-walled carbon nanotubes (MWNTs) emitting layer on two transparent ITO electrodes separated by an in-plane gap. When a conductive material was placed on top of the SiO₂ layer across the two bottom ITO electrodes,

electroluminescence was produced in the two overlapped areas. Interestingly, human fingers with natural conductivity (~ 300 to $1,000 \text{ } \Omega/\text{sq}$), can act as the floating electrode, so fingerprint detection and imaging can be achieved at every touch event with luminance of $2,000 \text{ cd/m}^2$ and a response time of 100 ms at 30 V and 100 kHz. The light intensity of the fingerprint increased with the applied voltage. Moreover, a light intensity of several hundred cd/m^2 was successfully maintained with a bending radius of 0.5 mm when the device was fabricated on a flexible PET substrate. Multiple bending cycles were performed, and negligible degradation of the performance was observed up to 1,000 cycles. Furthermore, the PLED arrays can be used for the position recognition of a finger touch, which is useful for personal privacy and public security applications.

To summary, flexible OLEDs not only have high colour contrast and efficiency for daily life requirements related to lighting or displays but can also produce a visual readout of medical sensing data. Introducing new electronic functions to the OLEDs has received considerable attention for health monitoring and information technologies. Therefore, flexible OLEDs will find more existing applications in the future.

3. Flexible OPV

The sustainable development of human society is increasingly recognized as a grand challenge in the 21st century. In particular, energy and environment have become two of the most prominent worldwide issues. As is well known, traditional energy sources, such as fossil fuels, still dominate the energy market, which has led to significant environmental contamination, such as the “greenhouse” effect and acid rain, from the release of carbon dioxide and toxic gases. Therefore, the growing world energy demand has urged people to seek new green and renewable alternatives to replace conventional fossil resources. Sunlight is an unlimited, clean and readily available energy source. Photovoltaic (PV) technology,

which harvests solar energy and converts it directly into electric power, is a promising way to alleviate the global energy crisis.

Organic photovoltaics (OPVs) have attracted tremendous attention as one of the rapidly developing PV technologies over the past two decades.^[113-118] Currently, the verified record OPV efficiency has reached over 13%.^[117] In virtue of the advantages such as light weight, low cost, mechanical flexibility and easily solution-processed fabrication,^[119-130] OPVs can be fabricated on flexible substrate. In particular, the large-scale roll-to-roll fabrication of flexible OPVs can be realized at room temperature, which is beneficial for commercialization. More importantly, lightweight and mechanically flexible OPVs have become of increasing interest for applications in portable devices, electronic fiber textiles, wearable electronics, synthetic skin, etc.

3.1. Materials

In this section, we review the development of active-layer semiconductors and electrodes applied in flexible OPVs. First, the properties of the active-layer materials are some of the most important determining factors in the overall performances of OPVs. Accompanied by innovations of novel donor and acceptor materials, the last two decades have seen the rapid development of semiconductors with strong and broadband absorption to improve the performance of OPVs. Because of the high crystallinity and relatively high hole mobility of poly(3-hexylthiophene) (P3HT) among the conjugated polymers, P3HT became the standard donor material for OPVs in the 2000s. Additionally, [6,6]-phenyl-C61-butyric acid methyl ester (PCBM) synthesized by Wudl et al.^[131], is one of the most important fullerene derivatives and is a widely used acceptor material even now. Although the first fabricated P3HT:PCBM-based cells possessed a PCE of only 2.8% in 2002, only 7 years later, in 2009, the highest reported efficiency of OPVs based on P3HT:PCBM improved up to 6.5%, as reported by Lee et al.^[132-135]

When further enhancement in the efficiency of OPVs, the obstacle of the narrow light absorption region of P3HT arose. To solve this bottleneck, in 2009, Yu et al. invented a new series of PBDTTT semiconducting polymers,^[136, 137] well known as PTB family, which possess a broad UV-vis absorption spectrum between 500 and 750 nm and a relative low bandgap. Afterwards, many conjugated-polymer donors were synthesized based on a backbone of alternating BDT and TT units.^[138-148] With variation in the alkyl and alkoxy side groups of PBDTTT, PBDTTT-E and PTB4 were reported to have improved V_{oc} values up to 0.76 V. Based on the model polymer PBDTTT-E, Hou et al.^[138] replaced the ester alkyl group on the TT unit by carbonyl alkyl (PBDTTT-C), resulting in much lower HOMO and LOMO levels. After molecular optimization, they then synthesized PBDTTT-CF based on PBDTTT-C, which showed an enhanced device efficiency of 7.73%,^[139] owing to a significant increase in the V_{oc} from 0.62 V to 0.76 V. On the other hand, after extensive structural optimization through another route, PTB7 was selected from the PTB family to blend with PC₇₁BM to create a new active-layer donor, giving a higher PCE of 7.4% for the first time with a significantly enhanced V_{oc} , J_{sc} , and FF of 14.5 mA/cm², 0.74V, 69.0%, respectively. The PTB7:PC₇₁BM-blend film exhibited a strong absorption wavelength range between 300 and 800 nm, demonstrating that PBDTTT-based polymers are a promising class of materials for application in high-performance OPVs. Following this research, OPVs with PCEs of over 8% were frequently reported based on the molecular design of PBDTTT polymers. The detailed photovoltaic parameters of some highly efficient (over 8%) single bulk heterojunction (BHJ) solar cells based on several well-known polymers:PC₇₁BM are listed in **Table 2**.

Although the excellent device performance of fullerene-based OPVs have been achieved, fullerene acceptors still exhibit some disadvantages, such as high-cost preparation, poor stability, complicated purification process, as well as weak absorption in the visible region. Recently, OPVs based on non-fullerene small-molecule acceptors have been developed as alternatives to fullerenes, which attracted a great deal of attention. Small-molecule materials

offer many advantages including low cost, good stability, easily tunable energy levels, and broadband absorption range.^[149-152] For example, in 2016, Zhan et al. reported that flexible OPVs based on a blend of non-fullerene small molecule acceptor IEIC with PTB7-Th via a roll-coating method under ambient atmosphere.^[153] The flexible OSCs fabricated on the ITO-free and ITO substrates showed highest PCEs of 1.79% and 2.26%, respectively, which were comparable to those of PCBM-based devices. Later, another small-molecule donor BDT2TR and the polymer acceptor PNDI-2T were studied by Lee et al. The devices based on BDT2TR:PNDI-2T showed remarkable photovoltaic results with a PCE of 4.43%, V_{OC} of 0.86 V, J_{SC} of 7.26 mA/cm², and FF of 71%.^[154] Particularly, the OPVs showed superior thermal and mechanical stability and thickness tolerance, and the flexibility levels of the devices were better than those of PC₇₁BM-based devices. In recent years, different research groups have made significant breakthroughs on the device performance of fullerene-free small molecule OPVs.^[155-159] Yan et al.^[152] reported that a low bandgap small molecule named IEIC offered complementary absorption when it was combined with PffT2-FTAZ-2DT. OPVs based on the fullerene-free materials led to a high PCE of 7.3% with extraordinary high V_{oc} up to 1.0 V. Later in 2016, Zhan and co-workers synthesized a planar fused-ring electron acceptor (IC-C6IDT-IC), which exhibited strong absorption in the wavelength region of 500-800 nm and high electron mobility of 1.1×10^{-3} cm²/Vs.^[160] The as-cast OPVs based on PDBT-T1:IC-C6IDT-IC without additional treatments yielded PCE of up to 8.71%, which is higher than those of most as-cast fullerene-based devices. More recently, higher PCE of non-fullerene OPVs were developed by Hou et al.^[118] The efficiency of fullerene-free OPVs based on PBDB-T:ITIC reached 11.2% with excellent thermal stability, outperforming that of fullerene-based devices. All of the recent breakthroughs suggest that, after molecular design and optimization, non-fullerene small-molecule donors and acceptors can be widely used in high-efficiency flexible OPVs.

All polymer OPVs using an n-type semiconducting polymer as the acceptor material instead of a fullerene, have been intensively studied recently. Comparing to fullerene-based OPVs, all-polymer solar cells have many advantages [24, 171-173]: i) Semiconducting polymers have high absorption coefficients in the visible wavelength range, while fullerenes have limited absorption. ii) The polymer energy level can be tuned easily, which can facilitate charge separation at the donor/acceptor interface. iii) All-polymer devices show low-cost fabrication and good thermal stability. However, the performance reported to date of the all-polymer solar cells composed of low-bandgap conjugated polymers has shown a much lower PCE of 5%~6% compared with that of the corresponding fullerene/polymer devices. The main limitations of the PCE of reported all-polymer OPVs are the relatively low J_{sc} (less than 14 mA/cm²) and FF (around 50%~60%) compared to those of fullerene/polymer devices.^[172, 173] Therefore, the development of novel semiconducting polymers is urgently needed to enhance the efficiency of the all-polymer solar cells. Recently, Jenekhe et al. reported all-polymer solar cells using PNDIS-HD:PBDTT-FTTE as the active-layer material.^[173] By controlling the polymer blend film self-organization rate through a simple film aging process at room temperature, a high PCE of 7.7% and a J_{sc} of 18.8 mA/cm² with an EQE of 85% were achieved. **Figure 4a** and **b** shows the band structure and absorption curves of the polymer donor and acceptor, respectively. Although the absorption bands of PBDTT-FTTE are mostly overlapped with those of PNDIS-HD, the polymer acceptor PBDTT-FTTE extends the light-harvesting region up to 800 nm, which makes the J_{sc} and EQE values superior to those of the corresponding PBDTT-FTTE:PC₇₁BM-based solar cells.

With the development of novel conjugated-polymer donors, fluorine substitution on the conjugated-polymer main chain has been demonstrated to be an effective approach for downshifting the HOMO level for a higher V_{oc} . In 2016, Li et al. addressed all-polymer OPVs based on the absorption-complementary polymer donor and acceptor of J51:N2200, which gave a record-high PCE of 8.27% and FF of 70.24% for all-polymer solar cells, by taking the

fluorinated medium-bandgap copolymer J51 as the donor and the low-bandgap polymer N2200 as the acceptor.^[174] Figure 4c and d shows the device structure of the all-polymer device and the optical absorption curve of the J51 film, N2200 films and polymer blend film, respectively. The complementary absorptions of the donor and acceptor polymers in the vis-NIR region were beneficial to the high photovoltaic performance of the devices. Additionally, the device with an active-layer thickness of 300 nm still demonstrated good photovoltaic performance with a PCE of approximately 4.5%. The thickness-insensitive photovoltaic properties of the all-polymer OPV are very important for the fabrication of large-area and flexible devices.

Organic-inorganic hybrid perovskite solar cells (PSCs) as one of the most popular research topics nowadays are promising candidates for replacing the conventional photovoltaics in commercial market due to their high absorption coefficient, long charge carrier lifetimes and competitive high efficiency. In the past few years, the PCEs of PSCs were rapidly increased from 3.8% to over 20%.^[175-181] Flexible PSCs have been fabricated on various kinds of flexible substrates, such as conducting plastic substrates, metal foils, ultrathin PET substrates, and even titanium fiber coil. The highest PCE of over 15% had been achieved for planar flexible PSCs on plastic substrates.^[181] With intensive investigation, it is believed that the PCE of flexible PSCs can be further improved very quickly. More importantly, the stability of flexible PSCs should be optimized, which is critical to practical applications in the future. Since PSCs cannot be regarded as standard organic electronic devices, we will not focus on this topic in this paper.

One advantage of the flexible OPVs compared to the conventional silicon solar cells is their possibility to be integrated into windows for buildings and automobiles. This requires the OPVs to possess two flexible and transparent electrodes. Currently, OPVs are typically fabricated on rigid glass substrates coated with ITO electrode. However, many inherent

problems, such as the limited abundance and increasing cost of indium, poor transparency, brittleness, and complicated fabrication process requiring the high-temperature crystallization of ITO films, make ITO a nonideal conductive electrode for flexible OPVs.^[182-184] Additionally, ITO can slowly release oxygen and indium into the buffer and active layer of the solar cells, which will result in the degradation of the device performance. In addition, the fragility of the ITO film prevents its large-scale application in OPVs. Therefore, it is necessary to develop other high-conductivity and transparent electrodes to replace ITO. One promising candidate is PEDOT:PSS, which is a polymer widely used in many conventional OPVs to extract holes due to its unique properties, such as high transparency, high conductivity, and easy processing. PEDOT:PSS is an aqueous solution with a mixture of two ionomers, PEDOT (polycation) and PSS (polyanion). According to the ratio of PEDOT and PSS, the deposited PEDOT:PSS film presents different conductivities. Currently, PEDOT:PSS materials with various additives are being studied as electrodes instead of ITO for flexible OPVs.^[184] Other techniques to improve the conductivity of PEDOT:PSS have also been systematically studied.^[185, 186] For example, Bradley et al. investigated the effects of thermal annealing, doping and post-treatment on the properties of PEDOT:PSS film.^[187]

Though OPVs based on transparent PEDOT:PSS anodes have demonstrated potential for application in flexible devices, the high acidity (pH~1) and hygroscopicity of PEDOT:PSS can result in instability and chemical reactions at the interface of PEDOT:PSS and the ITO electrode, as well as the introduction of H₂O into the active layer of the OPV, which further leads to degradation of the device performance.^[188-190] To solve this problem, carbon-based materials, such as two-dimensional (2D) graphene,^[191] reduced graphene oxide (rGO)^[192] and carbon nanotubes (CNTs)^[193] are being intensively investigated as electrodes in flexible OPVs due to their excellent flexibility, high transparency, high conductivity, and high chemical stability. Currently, graphene-based transparent electrodes have been successfully used in OPVs as bottom, top and all-graphene electrodes.^[121, 124, 194] Additionally, highly

conductive metal nanowires (NWs) or films, especially Ag NWs have also been considered to be good electrode candidates for the fabrication of flexible transparent OPVs.^[195, 196]

3.2. Device fabrication and performance

Based on different semiconductors and electrodes mentioned before, in this section, the fabrication processes and device performances of various flexible OPVs are reviewed. As early as 2008, Hau reported a flexible inverted OPV based on P3HT:PCBM with ITO, showing a PCE of 3.3%.^[197] Later, in 2010, Wang presented that at relatively low temperature, the PCE of flexible P3HT:PCBM-based OPVs with inverted structure could be improved to 4.18% with optimization of the ZnO electron-transporting layer (ETL).^[198] It is noteworthy that Martin et al. presented an ultrathin, light, and flexible OPV fabricated on 1.4- μm -thick PET substrates in 2012.^[199] The devices based on P3HT:PCBM using a high-conductivity PEDOT:PSS electrode replacing ITO showed a PCE of over 4%. As depicted in **Figure 5a**, the total device was only 1.9 μm thick and had high flexibility. Using the ITO-free architecture on PET, they obtained comparable efficiency and demonstrated the excellent mechanical properties of the device. The extreme bending flexibility of the solar cell is illustrated in Figure 5b and 5c. The scanning electron microscopy (SEM) image of the compressed solar cell in Figure 5d highlights the random network of wrinkles with extremely small bending radii. The durability of the devices under repeated stretching and compression was also investigated. They cycled the device from 0% (original size) to 50% quasi-linear compression and back more than 20 times. At each cycle, the *I-V* characteristics were measured, both in the compressed and extended state, as shown in Figure 5e. The cycling test showed a gradual decrease in the I_{sc} , *FF* and PCE, resulting in a 27% decrease in power after 22 cycles, and the normalized device parameters at each cycle (extended) are shown in Figure 5f. This lightweight power source has many potential applications in remote sensing systems, disposable use, etc.

With the rapid development of high-efficiency polymer donor materials, the efficiency of flexible fullerene-based OPVs has also been significantly enhanced. Wu et al. fabricated a flexible OSC with the device structure of PET/ITO/ PEN/PTB7:PC₇₁BM/MoO₃/Al.^[183] As depicted in **Figure 6a**, comparison of the optical transmittance between PET/ITO and glass/ITO substrates indicated that the PET/ITO substrate possesses high optical transmittance. As shown in **Figure 6b**, the PCE of the device reached 8.7% with V_{oc} , J_{sc} , and FF of 0.74V, 17.94 mA/cm², 0.659, respectively. The alcohol-water-soluble conjugated polymer poly [(9,9-bis(30-(N,N-dimethylamino) propyl)-2,7-fluorene)-alt-2,7-(9,9-dioctylfluorene)] (PFN) as a new ETL could smooth the surface morphology of the active layer and decrease the work function of PET/ITO for efficient electron extraction. **Figure 6c** showed the flexible OPV with a certified efficiency of 8.7%.

Moreover, a tandem flexible OPV was fabricated by Chang et al., as shown in **Figure 6d**.^[200] They applied a TBAI-doped cross-linked PCBN3 film as the ETL in an OPV, which could deliver several remarkable features, including easy solution processability, good ambient and chemical stability, and fine-tunability of the work function of the electrode. The rigid device G based on a front cell with the wide-bandgap material P3HT:ICBA and a rear cell with the low-bandgap material PSBTBT:PC₇₁BM on a glass substrate gave a high PCE of 9.3%, with a J_{sc} of 9.25 mA/cm², V_{oc} of 1.45 V, and FF of 68.97% (**Figure 6e**). The flexible tandem solar cells, device H, using ITO-coated PEN as the substrate, delivered a high PCE of 8.7% with J_{sc} of 8.80 mA/cm², V_{oc} of 1.47 V, and FF of 0.671. The relatively lower PCE can be attributed to the higher ITO sheet resistance on the PEN plastic substrate and lower optical transparency. Under low light intensity, the PCEs were improved up to 10.1% and 9.2% for the devices on glass (device I) and PEN substrate (device J), respectively (**Figure 6f**).

More encouragingly, Kim et al. found that the all-polymer active layer demonstrated significantly enhanced flexibility compared with polymer/PCBM devices.^[172] They developed

a high-efficiency and mechanically flexible all-polymer OPVs based on PBDTTTPD donor and P(NDI2HD-T) acceptor. This type of OPV exhibited a PCE of 6.64%, which was higher than that of PBDTTTPD:PCBM-based solar cells, which showed a PCE of 6.12% (**Figure 7a,b**). Moreover, the all-polymer blend films exhibited superior flexibility, stretching and bending properties. The experimental results in Figure 7c and d show that the all-polymer solar cells have far superior mechanical durability to fullerene OPVs. Comparing the SEM morphology of the two types of OPVs, obvious crack propagation was observed in the fullerene-based film due to mechanical deformation (Figure 7e), while there was no change in the morphological properties of the all-polymer film (Figure 7f). Furthermore, the 60- and 470-fold improvements in elongation at break and toughness, respectively, make the all-polymer OPV a much better candidate for applications in flexible and portable devices.

As mentioned before, to enhance the conductivity of PEDOT:PSS, additives or treatments are widely used in the device fabrication process. Kim et al. achieved high-conductivity PEDOT:PSS (PH500) as a polymer anode on both glass and flexible plastic substrates by doping with 5% DMSO.^[184] The efficiencies of the ITO-free OPVs based on P3HT:PCBM on glass and flexible plastic substrates were 3.27% and 2.8%, respectively. It was demonstrated that the conductivity of H₂SO₄-treated PEDOT:PSS could be effectively improved. By utilizing a transfer-printing method, Kim et al. fabricated the H₂SO₄-treated PEDOT:PSS with a high conductivity of 4380 S/cm and high transmittance in the visible region (>90%) on a PEN substrate.^[201] Flexible OPVs based on the modified electrode and PTB7-Th:PC₇₁BM active layer exhibited a PCE of 7.7%, which is nearly identical to that of conventional ITO-based OSCs. More importantly, the flexible device showed excellent bending durability and could retain over 90% of its initial PCE after 1,000 bending cycles at a radius of 1 mm.

For the application of 2D carbon-based materials as electrodes in flexible OPVs, Acro et al. investigated flexible OSCs with CVD-growth graphene as the bottom transparent

electrode,^[191] which gave the maximum PCE of 1.18% and better bending stability than traditional devices based on ITO electrode. Yin et al. also presented a flexible OPV based on highly reduced GO as the transparent anode with P3HT:PCBM as the active layer.^[192] The devices gave a maximum efficiency of 0.78% and retained 70% of their initial PCE after 1,600 bending cycles. In our previous work,^[121] a highly doped multilayer graphene anode was applied in the flexible OPVs on PI substrates (**Figure 8**). The transmittance of different layers of graphene films is shown in Figure 8a. Comparing with the ITO transparent electrode, the transmittance decreased only 2.3% in the visible range for a single layer of graphene. For the four-layer graphene film, the transmittance remained at approximately 90%. Multilayer graphene top electrodes were used in P3HT:PCBM-based devices with a structure of graphene/PEDOT:PSS/P3HT:PCBM/ZnO/Ag/PI. The *J-V* curves in Figure 8b exhibit the performance of the OPVs with 1 to 4 layers of modified graphene. The device with the 2-layer graphene electrode exhibited an optimum PCE of up to 3.2%, resulting from V_{oc} of 0.597 V, J_{sc} of 10.6 mA/cm², and *FF* of 50.1%. When fabricated on a thin PI substrate (thickness of 50 mm), the device showed excellent bending stability, and its PCE decreased only 8% after 1,000 bending cycles with a curved radius of approximately 3 mm, as shown in Figure 8c. More importantly, multilayer graphene has a packaging effect on flexible OPVs, which can substantially improve the device stability in air (Figure 8d). It is notable that the flexible OPVs with graphene top electrodes may not need additional packaging, which will simplify device fabrication, enhance flexibility and decrease the cost of the devices.

In addition, Rowell et al. fabricated flexible transparent conducting electrodes by printing films of single-walled CNT (SWCNT) networks on plastic substrates and demonstrated their use as transparent electrodes for efficient, flexible OPVs based on P3HT:PCBM.^[202] The device displayed a PCE of 2.5% with rather smooth and homogeneous CNT films, showing a transmittance of 85% at 550 nm and a sheet resistance of 200 Ω /sq. In addition, they further demonstrated that the flexibility of the devices is far

superior over the devices using ITO/PET flexible electrode. More recently, Jeon et al. reported MoO_x-modified CNTs, where the MoO_x/CNTs worked as an electron-blocking transparent electrode when applied in PTB7:PC₇₁BM-based OPVs.^[193] The dual functionalities of MoO_x/CNTs lead to a PCE of up to 3.91% for flexible OPV fabricated on PET substrates and the capability to withstand a severe cyclic flex test.

You et al. studied a flexible OPV based on PBnDTDTffBT:PCBM with a Ag NWs/PET electrode prepared by a simple solution-processing method.^[195] They found that the bending durability of the flexible devices led to 90% retention of their initial efficiency after 10 bending cycles. In 2012, Yang et al. reported another flexible OPV with a two-fold improved efficiency of 4% based on PDBTT-DPP:PC₆₁BM with a Ag NW-based composite as the transparent top electrode.^[196] By carefully selecting the length of Ag NWs, Song et al. prepared a Ag NWs/PEDOT:PSS composite electrode that possessed a reduced sheet resistance. With the modified electrode, flexible OPVs based on photoactive layer of PTB7-F20:PC₇₁BM showed a high PCE of 5.02%.^[203] Moreover, Seo et al. presented a novel cold isostatic pressing technique at room temperature to prepare transparent Ag NW electrodes^[204] that showed outstanding electrical and optical properties. As shown in **Figure 9a,b**, the flexible OPVs based on PTB7-Th:PC₇₁BM with the novel Ag NWs electrode exhibit a PCE of 8.94% on glass and 8.75% on a PET substrate. This flexible device also exhibited excellent bending durability, maintaining 95.5% of the initial PCE after 1,000 bending cycles for a bending radius of 4.8 mm. A semitransparent ultrathin metal film-Ag (UTMF-Ag) can also be integrated into the flexible OPVs. In 2015, Yu et al. designed a microcavity architecture of UTMF-Ag,^[205] which is regarded as an enhanced light-trapping configuration as is depicted in **Figure 9c**. They demonstrated an OPV based on PBDTT-F-TT:PC₇₁BM with the UTMF electrode with a significantly increased J_{sc} of 18.30 mA/cm² and PCE of 10.5% over those obtained from its ITO counterpart (**Figure 9d**). When the active-layer area was enlarged to 1 cm², the devices still afford a high PCE of 7.21%, which is approximately 26% improvement

over that of the ITO-based device. These innovative strategies provide a promising solution to further develop highly efficient, large-area, and flexible OPVs.

4. Flexible OTFTs

OTFTs are fundamental components behind various organic electronics that can act as switches, drivers, amplifiers, transducers, data-storage components, etc. Typical OTFTs are three-terminal electronic devices consisting of an organic semiconducting layer, a gate dielectric layer and three electrodes (source, drain, and gate). Two current states, namely, an “ON” state with high channel current (I_{DS}) and an “OFF” state with low channel current, can be effectively switched by applying a gate voltage (V_{GS}). Compared with the traditional counterpart of silicon CMOS transistors, OTFTs can be manufactured directly onto a variety of flexible and large-area substrates at low processing temperatures.^[2] It has been recognized that OTFTs are not only essential building blocks for the next generation of low-cost and large-area flexible organic circuits, such as displays and radio-frequency identification (RFID) tags, but also promising transducers for disposable physical/chemical/biological sensors.

4.1. Materials

High-mobility OSCs are the core materials of flexible OTFTs. The charge-carrier mobility (μ) directly depends on the chemical structure of the conjugated frameworks and the intermolecular (or interchain) π -orbital overlap in the OSCs. The majority of OSCs are p-type materials for both small-molecule and polymer semiconductors. Currently, p-type small-molecule semiconductors, including pentacene, rubrene, benzothiophene (C8-BTBT) and derivatives (C_n-BTBT), dinaphtho[2,3-b:2',3'-f] thieno [3,2-b] thiophene (DNNT) and derivatives,^[206] can show a standard hole mobility of 1–10 cm²/Vs, which is higher than that of amorphous silicon (0.5–1.0 cm²/Vs). For DNNT or C_n-BTBT systems, mobilities higher than 10 cm²/Vs have been reported, depending on the fabrication methods of OTFTs.^[207, 208] Specifically, some small-molecule OSCs, such as C8-BTBT, DNNT, triisopropyl-silylethynyl

pentacene (TIPS-pentacene), and 2,8-difluoro-5,11-bis(triethylsilylethynyl)anthradithiophene (diF-TESADT), could be deposited on substrates through solution-assisted methods.^[209] This feature makes it possible to improve the crystallization and uniformity of organic films by blending soluble small-molecule OSCs with low-permittivity (low- k) polymeric matrix.^[210]^{211]} Although evaporated and highly-purified small-molecule semiconductors tend to have higher mobilities than their polymeric counterparts and printed OSCs, they are sensitive to microstructural defects created by mechanical strain, for the intermolecular distances at different bending states play a crucial role in charge transport.^[212] The key performance metrics of polymeric OSCs are their low-temperature processing properties and better mechanical flexibility. At present, polymeric OSCs with the highest mobility are predominantly donor-acceptor (D-A)-type copolymers with a hole mobility exceeding 1 cm^2/Vs , such as indacenodithiophene-co-benzothiadiazole (IDT-BT), cyclopentadithiophene-benzothiadiazole (CDT-BTZ), PCDTPT, DPP-based polymers and isoindigo-based polymers.^[213, 214]

Ambient-stable n-type and ambipolar OSCs are highly desirable for realizing flexible ambipolar transistors, p-n junctions and organic complementary circuits.^[215] The electron mobility of typical n-type small molecular OSCs have reached over 0.5 cm^2/Vs , and examples include the naphthalene tetracarboxylic diimides (NDI)-based NDI3HU-DTYM2 and perylene tetracarboxylic diimides (PDI)-based materials.^[216] The well-known n-type polymer P(NDI2OD-T2) has a high electron mobility of 0.85 cm^2/Vs even under ambient conditions.^[217] In comparison with the unipolar OSCs, ambipolar OSCs, which can transport both hole and electron charge carriers in one OTFT device, are important for the simple fabrication of complementary integrated circuits without requiring advanced patterning techniques to deposit individual p- and n-type OSCs.^[50, 218] Diketopyrrolopyrroloethieno[3,2-b]thiophene (DPPT-TT) is one of the most commonly used ambipolar polymer OSCs with both hole and electron mobilities exceeding 1 cm^2/Vs .^[219] Apart from designing new

conjugated frameworks, the incorporation of small-molecular additives^[220, 221] or graphene^[222] into conjugated-polymer films has also been explored to increase charge-carrier mobility. However, it is notable that the extraction of carrier mobility is based on an ideal field-effect transistor (FET) model without the consideration of OTFT performance deviation from an ideal FET.^[223, 224] Microscopic understanding of charge transport physics, e.g., the inherent structural and electronic disorder in thin organic semiconductors, is also crucial to reliable mobility extraction in OTFTs.

In an OTFT, a conduction channel is formed through a few semiconducting molecular layers at the semiconducting-dielectric interfaces. Generally, 2-3 molecular layers are crucial to obtaining reliable device operation. The performance of flexible OTFTs also depends on the properties of dielectrics and the interfacial compatibility between the semiconductors and dielectrics. Normally, a smooth and hydrophobic dielectric-semiconductor interface is critical for semiconductor growth, charge transport and device stability. The effect of strain on the dielectric material composition is reported to be governed by the relative change in the surface energy of the dielectric material.^[225] Conventional inorganic dielectrics are fragile and usually require harsh vacuum deposition techniques or high-temperature processes.^[226] Various amorphous polymer insulators have been used as soft gate dielectrics. Among them, nonpolar ($k < 3.5$) polymers can be used in both n-type and p-type OTFTs, typical examples are CYTOP (2.1), PS (2.6), PaMS (2.6), PI (3.4), Parylene (3.0), and PMMA (3.5). Polar ($k > 5$) polymers are preferable for p-type OTFTs,^[227] such as poly(vinyl alcohol) (PVA, 7.3) and relaxor ferroelectric polymer poly(vinylidene fluoridetrifluoroethylene-chlorofluoroethylene) [P(VDF-TrFE-CFE),^[228] >60]. Note that low-operating voltages are essential for low-power OTFTs in flexible electronic skins and wearable devices. Generally, a high- k dielectric with low thickness is required to reduce the operating voltage. In addition, self-assembled monolayers (SAMs) have also been developed as a powerful platform for the interface engineering of OTFTs.^[229] In addition to the pristine polymer, control over the different

polymer components to form bilayer or composite dielectrics can be used to enhance the mechanical compatibility and adhesion energy between semiconductor layer and dielectric layer for stretchable or self-healing OTFTs.^[230-233]

An ohmic contact between the electrode and the OSC determines the effective charge injection in the OTFT. By using electrode materials with suitable work function and choosing an appropriate device structure (top gate or bottom gate), one can obtain OTFTs with low contact resistance. Noble metals or oxide electrodes are not suitable for flexible devices due to their high Young's modulus. Naturally, flexible electrodes including conducting polymers (PEDOT:PSS, CB[8]^[26]), functionalized metal nanostructures (Ag NW^[234], Cu NW,^[20] Ag flake), or carbon-based materials (graphene, SWNTs, MWNTs^[235]) are more suitable as inks for printed flexible OTFTs. To realize elastic electrodes, a very high conductivity ($>10^3$ S/cm) and large mechanical deformation (strain $>10\%$) can be achieved by infiltrating highly conductive nanomaterials into elastic matrix materials, such as rubber, PDMS and polyurethane (PU).^[236, 237] Moreover, soft conducting biocompatible gel materials are promising for use in implantable electronic system.^[235]

Lowering the process temperature can broaden the range of substrate choices to include low-cost plastic films, rubber, textiles and even paper. Hu et. al ^[238] reported highly transparent and flexible OTFTs fabricated on properly designed nanopaper. When measured during bending, the nanopaper tends to self-assemble into a layer-by-layer structure, which can effectively release the strain when the nanopaper is bent. Only a 10.2% and a 9.8% decreases in mobility were observed when the device was bent in the direction parallel to the conduction channel direction and vertical to the conduction channel direction, respectively.

4.2. Flexible Organic Circuits

OTFTs are key logic units of flexible integrated circuits (ICs), ranging from small circuits of inverters, ring oscillators, rectifier, or amplifiers to more complex microprocessor.^[239] Beyond

this, OTFTs enable the dominant use of drivers in flexible active-matrix flat-panel displays and radio-frequency identification (RFID) tags. Printed OTFTs are crucial for the realization of the low-cost and fast R2R manufacturing of flexible displays and RFID tags. The parameters need to be considered include the transconductance (g_m), mobility, on/off ratio, subthreshold swing (SS), and threshold voltage (V_{th}),^[240] which are determined by the crystallinity of the semiconductor ink, the specific capacitance of the gate dielectric and the inverse of the channel length.^[241] However, two major problems, including high operational voltages and instability during operation and storage, commonly found in OTFTs should be solved in practical applications.^[242]

RFID technology has been widely used in access control systems and food safety traceability.^[243] Flexible RFID tags with sensing capabilities can be attached to objects to not only allow their identification at different locations but also obtain information about their quality or the environment in which they are placed. To realize circuits with higher integration levels, the integration of both n- and p-type OSCs enables the fabrication of complementary circuits that are characterized by better speed and reliability than their unipolar counterparts.^[244] Both the electron and hole mobilities of the individual printed OTFTs should be high ($>1 \text{ cm}^2/\text{Vs}$) to realize high-speed circuitry needed for applications such as near-field communication (NFC) operated at 13.56 MHz.^[245] Palmisano et al.^[246] presented the first printed organic 13-MHz RFID using an organic complementary OTFT technology on a PEN substrate. An n-type OSC (Polyera ActivInk) and p-type OSC (Merck Lisicon S1200) were patterned by printing methods. A common fluoropolymer dielectric (Merck Lisicon D139, 750 nm thickness) was then screen-printed on top of both semiconductors, and finally, a silver-ink conductor was screen-printed to form the gate electrode. With more than 250 transistors on the same foil, the functionality of this organic RFID was demonstrated at the internally generated supply voltage of 24 V for a reading range of 2-5 cm and a bit-rate up to 50 bit/s. To achieve their full potential for item-level tagging on all goods, a R2R inline

printing process to print all the units of the passive RFID tag was considered as an alternative to current Si-based technology.^[247] Cho et al.^[248] have employed a R2R gravure printer with two printing units to fabricate an all-printed tags on PET, in which surface-modified SWCNT inks with intrinsic high mobility and stability were used to print the active layers. The 1-bit tag has an estimated cost of 0.03 dollar/unit and can generate 102.8 Hz of clock signal as the tag approaches the 13.56-MHz RFID reader. Tags with sensor functionality for packaging monitoring can minimize the number of discrete components that are integrated into the RFID system, which is crucial to further reduce its cost per unit. For this, Falco and co-workers^[249] presented a printed passive RFID tag integrating one temperature sensor and a printed OPD (**Figure 10a**). The whole tag was able to provide two environmental parameters, light intensity and temperature, and was suitable for supply chain control and monitoring.

For flexible displays, compared with passive-matrix OLEDs, active-matrix OLED (AMOLED) displays, in which the pixels are driven and switched by OTFTs, have received considerable attention. AMOLED technology consumes less power and can display better performance in terms of easily achieving high brightness and high resolution, which is more conducive to OLED colorization.^[252] As an OLED is a current-driven device, its brightness is proportional to the amount of current. To drive a flexible OLED display, stable OTFT performance in the cyclic bending state is key. Significant concerns remain about the operational and environmental stability of AMOLEDs resulting from a change in the OLED current caused by a V_{th} shift of the OTFT, which directly affects the panel luminance characteristics. In this regard, the transfer characteristics of environmentally robust flexible OTFTs with a typical deviation in the on current of less than 5% are required for realization of the uniform luminance of each pixel. Additionally, to satisfy the luminance specification with respect to visibility, a high mobility is necessary to achieve a high current on/off ratio at lower power consumption.^[253] State-of-the art OSC materials that have allowed the realization of OTFTs with high mobilities $>1 \text{ cm}^2 / \text{Vs}$, which may approach the mobility requirements to

address OLEDs.^[254] Noda et al. reported on OTFT-driven rollable OLED display (Figure 10b)^[250] in which a *peri-xanthoxanthene* (PXX) derivative was used for the active layer of the OTFT backplane. The variation in V_{th} in this OTFT was negligibly small during a 1,500-sec DC bias stress test. Under compressive bending, the mobility increased with decreasing bending radius, while the mobility decreased with decreasing bending radius under tensile bending, and this change was reversible. The change in mobility was less than 5% with a bending radius of 3 mm under both bending directions, which enables the operation of flexible displays. As a result, the display could be repeatedly rolled up and released along a 4-mm cylinder 1,000 times, and no line defects, dark spots, or bright spots were observed. Being transparent for both OLEDs and OTFTs significantly expands the range of applications of AMOLED displays. Pei and co-workers^[251] reported a fully stretchable and transparent OTFT suitable for stretchable AMOLEDs. The OTFT driver employed a Ag NW-PU acrylate (PUA) composite as the stretchable transparent electrodes, a SWCNT network as the channel and a PU-co-polyethylene glycol (PU-co-PEG) as the elastomeric dielectric. The stretchable OTFT showed a mobility of $\sim 30 \text{ cm}^2/\text{Vs}$, on/off ratio of 10^3 - 10^4 , and switching current $> 100 \mu\text{A}$ and can be stretched by up to 50% strain and subjected to 500 cycles of repeated stretching to 20% strain without significant loss in electrical properties (Figure 10c,d). This flexible OTFT was successfully adapted to switch a stretchable white-light OLED from totally dark to 196 cd/m^2 at 8 V, and a luminance of 63 cd/m^2 could be maintained even when stretched up to 30% strain (along the channel length direction).

4.3. Flexible Sensors

Over the past several years, exciting work have been done to develop high-performance flexible sensors for wearable human-activity/environmental monitoring, process control, and personal healthcare.^[255, 256] Owing to the inherent functionality of signal transduction and amplification, solution-processing capacity and ease of miniaturization/integration, OTFTs

serve as an ideal platform for high-performance biosensor, photosensor, gas sensor and stress sensor.^[257] The general sensing mechanism is as follows: when a device is or is not in contact with the analyte (normally liquid, gas, light, force, etc.), the drain current (I_{DS}) flowing through the channel can be significantly modulated due to physical, chemical or biological reactions on the device, resulting a readable or recordable response signal. The sensing performance, including sensitivity, limit of detection (LOD), response time, etc., are strongly determined by the device structure, the active layer and the channel interfaces (**Table 3**).^[258] According to the relative placement of the gate electrode and active layer, there are two basic configurations of OTFTs: bottom gate and top gate. Both device structures have unique features that can be used to meet different sensing demands. For example, the bottom gate geometry is far more utilized in gas sensors in which the semiconducting layer is directly exposed to air, such that the vapor-phase chemical can approach the transistor channel region embedded at the bottom of the OSC film.

4.3.1. Biological Sensor

Biosensors can convert biochemical signals into electronic signals. The sensing of various biological substances (DNA, glucose, protein, cells, etc.) and signals (wrist pulse, blood pressure, cell activities, nerve impulse, etc.) using flexible OTFT-based sensors has been actively researched to enable continuous health monitoring, drug delivery and cell control.^[259] Organic field-effect transistors (OFETs) are traditional solid OTFTs in which the channel modulation is produced by a capacitive field-effect mechanism. OFET-based biosensors are used most intensively for DNA sensing in dry conditions and are disposable once the semiconductor layer (e.g., pentacene) is corroded by the buffer solution. However, aqueous solution is the natural environment for biological targets, and the concentration of biological species is normally very low. In this regard, a novel electrolyte-gated OFET (EG-OFET) sensor was developed, which has an ion-sensitive field-effect transistor (ISFET)-like configuration.^[260] For the EG-OFET architecture, the OSC layer is in ionic contact with a gate

electrode *via* an aqueous electrolyte. When a gate voltage is applied, two electrical double layers (EDLs) with high capacitance (a few to a few tens of $\mu\text{F}/\text{cm}^2$) are formed at both the electrolyte-gate interface and electrolyte-semiconductor interface, respectively.^[261] As a result, the EG-OFET-based biosensor can operate at low gate voltage (approximately 1 V), which has been used for *in situ* DNA sensing. Furthermore, when an OSC layer (e.g., PEDOT:PSS, polypyrrole (PPy), or polyaniline (PANI)) can be electrochemically doped in an electrolyte under a bias voltage, another ISFET-like biosensor, called organic electrochemical transistor (OECT), is constructed. Different from EG-OFETs, the operation mechanism of OECTs is based on the reversible electrochemical doping/de-doping process occurring in the OSC layer.^[262] OECTs can work stably in aqueous environment at lower working voltages and allow label-free detections. Both EG-OFETs and OECTs have advantages of high sensitivity, good selectivity and superior biocompatibility for real-time chemical/biological sensing applications. In addition, they have very simple structures and can be easily fabricated on different flexible substrates by solution-processing techniques. However, there is debate about whether the channel current changes of EG-OFETs are majorly induced by field-effect doping or electrochemical doping. In this section, we will briefly present recent advances in OECT-based flexible biosensors.

PEDOT:PSS is one of the most successful electrically conducting polymers due to its high air stability, high electrical conductivity and biocompatibility. However, PEDOT:PSS is quite rigid with an elastic strain limit of only 2%.^[263] To achieve flexible and stable OECTs, our group has developed a plastic strain gauge using strong-acid-treated PEDOT:PSS films embedded into PDMS, which demonstrated a high conductivity of 2890 S/cm and an enhanced stretchability of 20% strain.^[264] Cicoira et al. mixed PEDOT:PSS with a biocompatible conductivity enhancer glycerol.^[265, 266] This functional PEDOT:PSS film shows a conductivity of ~600 S/cm and robust adhesion on PET substrates. After 500 bending cycles, the current loss is less than 4%. When further mixed with a third hydrophilicity enhancer

(Capstone FS-30), this functional conducting polymer can be spin-coated on a 30% pre-stretched PDMS substrate to enable a stretchable OECT.

Various strategies have been developed to improve the sensitivity of OECTs. Highly sensitive enzyme sensors have important applications in the diagnosis of diseases. Cicoira et al.^[267] investigated the influence of device geometry on OECT-based enzymatic sensors. They demonstrated that the sensitivity of the device increased as the gate size decreased. Berggren et al.^[268] reported the blending of PEDOT:PSS conducting layer with Pt NPs for glutamate and acetylcholine sensing. The detection limit of the device is a few μM . Our group modified a Pt gate electrode with enzyme and nanomaterials, such as Pt NPs and multi-wall CNTs (MWCNT).^[269] The detection limit of the device could be extended to 5 nM range. However, the above-mentioned devices are not flexible. Apart from high sensitivity, the selectivity of a biosensor is of great importance to its practical applications. However, the device selectivity has been rarely studied in OECT-based biosensors. Guo et al.^[270] presented a flexible and selective OECT sensor for noninvasive cancer cell identification. The device was based on screen-printed carbon source and drain electrodes on PET substrates and poly (3-aminophenylboronic acid) (PABA)-modified glass carbon gate electrodes. The device showed the capacity to identify cancer and normal cells in a simple and noninvasive way, and the detection limit was 8 μM . In 2015, our group demonstrated high-performance flexible OECT-based enzyme sensors with a detection limit of 10 nM.^[271] The selectivity of the devices was effectively improved by coating a PANI/Nafion-graphene bilayer on the gate electrode. This flexible OECT can be attached to various deformable surfaces (**Figure 11a**) and showed stable performance over up to 1,000 bending cycles (**Figure 11b**). Interestingly, this OECT can be used for testing the glucose level in saliva (**Figure 11c**), which provides a viable method for noninvasive glucose detection.

Benefiting from the compatibility with ongoing miniaturization techniques, OECT can be integrated into microfluidic systems to achieve real-time detection and high-throughput

sensing.^[274, 275] Recently, Owens et al.^[275] reported the coupling of OECTs with microfluidics to achieve a multi-parametric transducer platform based on PEDOT:PSS channels. Laminar flow can be used to apply a mechanical shear stress to live cells. This device could provide real-time, multi-parametric information on cell integrity from *in vitro* monitoring. Our group demonstrated a label-free DNA sensor by using a PEDOT:PSS-based OECT integrated in a microfluidic system on a PET substrate.^[276] The device showed little difference in performance under outcurve/incurve bending states. The device could detect complementary DNA targets down to 1 nM. In addition, the detection limit was extended to 10 pM when the hybridization of DNA was enhanced by applying an electric pulse to the gate electrode. It is expected that this kind of “lab-on-chip” system could have promising applications in highly sensitive biosensors.

Electrical impulses accompany many daily activities of our bodies, and abnormalities in these physiological signals are related to severe diseases. Owing to their mechanical flexibility and biocompatibility, flexible OECTs with PEDOT:PSS active layers have emerged as versatile platforms for various biological signal sensing, monitoring and clinical applications.^[277] In addition, the entire thickness of the porous conducting polymer layers is involved in electrochemical interactions with ions, which gives OECTs high g_m (typically over 1 mS) and a fast response speed of ~ 1 kHz for detecting considerably small electrophysiological signals.^[278] Additionally, a high signal-to-noise ratio (SNR) is required to achieved a shorter recording time to obtain electrophysiological information. Recently, flexible OECT-based active multielectrode arrays (MEAs) were developed for local signal amplification and high spatial resolution. Hsing et al.^[279] fabricated a PEDOT:PSS-based MEA for monitoring action potentials from cardiomyocyte-like HL-1 cells. Each OECT had an active area of $30 \times 40 \mu\text{m}^2$ and was separated by a distance of $200 \mu\text{m}$ from the other OECTs. PDMS was chosen as the cell culture chamber to maintain the flexibility of the whole device. The as-fabricated device had a large g_m of up to 2.5 mS and could maintain an excellent SNR

of ~4 dB under different bending strains owing to the flexible nature of PEDOT:PSS. To enable optogenetic neural signal recordings, Wonryung et al.^[273] manufactured a transparent and active MEA consisting of transparent OECTs (Figure 11d,e). The 2×2 array of PEDOT:PSS-based OECTs was manufactured with a total thickness of $3 \mu\text{m}$ on a parylene substrate, where each OECT exhibited a large g_m of 1.1 mS and a fast response time of $363 \mu\text{s}$. This transparent and active MEA was demonstrated by mapping electrocorticography (ECoG) signals upon blue laser stimulation with 1-mm^2 spatial resolution and a SNR of 13 dB. To achieve high spatial and temporal resolution, Someya and co-workers^[272] demonstrated an ultraflexible 3×5 electrophysiology array by integrating OECTs and OFETs for dynamic monitoring of a rat's gracilis muscles (Figure 11f). The integrated devices had an ultralow thickness of $2.0 \mu\text{m}$ and exhibited good conformability and negligible mechanical interference. The g_m was larger than 2.5 mS and was practically unchanged before and after crumpling. The device exhibited a 4-mm^2 spatial resolution and 3-kHz temporal resolution and could detect the electromyogram with a time resolution of 1 ms or less. Owing to their stable performance when in good mechanical contact with 3D curved biological surfaces, flexible OECT arrays pave the way for realizing inexpensive, disposable *in vitro* and *in vivo* monitoring chips.^[280, 281]

4.3.2. Photo Sensor

An organic phototransistor (OPT) is a type of photo detector in which the incident light signal can modulate the charge-carrier density in the active channel of OTFTs, thereby changing the channel conductance.^[282, 283] Compared to conventional photodiodes, OPTs detect the light signal more sensitively, and they are easily incorporated in electronic circuitry because of their CMOS-like configuration.^[284] The spectral sensitivity of organic photosensitive materials can be modified to be panchromatic or selectively tuned to a specific wavelength from ultraviolet to near-infrared (NIR) by controlling their molecular structures.^[285] Along

with their inherent flexibility, OPTs are lightweight and compatible under nonplanar sensing conditions, which are promising for emerging applications such as artificial retina, optical communications, medical imaging, night surveillance and wearable healthcare facilities.^[286-289]

The physical processes of OPTs are composed of exciton generation, exciton diffusion, exciton dissociation and transport of the resulting free charge carriers. Conjugated-polymer OSCs suffer from the intrinsic limitation of high exciton binding energy (0.2-1 eV). The heterojunction strategy has been successfully utilized as a complementary light absorber, in which sufficient energy offsets can effectively separate tightly bound excitons at p-n junctions.^[290] Traditional heterojunction materials mainly use small molecules, which are not suitable for solution processing or flexible substrates. Organometal halide perovskites have emerged as promising optoelectronic materials, as their low-temperature fabrication process makes them compatible with flexible substrates. Most recently, our group reported a high-gain and flexible broadband photosensor based on perovskite ($\text{CH}_3\text{NH}_3\text{PbI}_{3-x}\text{Cl}_x$)/PEDOT:PSS vertical heterojunctions on PI substrates (**Figure 12a**).^[291] Within this hybrid structure, perovskite served as the light-absorbing medium due to its exceptional light absorption capabilities, wide-range tunable bandgap and microscale carrier-diffusion length^[292, 293], while PEDOT:PSS functioned as the effective hole-transport channel. At a low operating voltage of only 0.5 V, the device demonstrated a high responsivity (R) of $\sim 10^9$ A/W and a specific detectivity of $\sim 10^{14}$ Jones over a broadband spectrum ranging from ultraviolet to near-infrared. The performance showed little change after 300 bending cycles (**Figure 12b,c**), indicating its potential application in wearable and flexible electronics. Stretchable OPTs can be used to develop wearable biological systems for medical applications. Omnidirectionally stretchable OPTs are limited by difficulties in designing material and fabrication processes that enable stretchability in multiaxial directions. Lee et al. proposed a new approach involving an organic-inorganic p-n heterojunction photodetector comprised of free-standing ZnO nanorods grown on a PEDOT:PSS transport layer.^[286] The above

components were coated on a 3D micropatterned stretchable substrate containing bumps and valleys. This structure allows the device to accommodate large tensile strain in all directions. As a result, the stretchable UV photodetectors exhibited good stability when subjected to uniaxial and multiaxial strains of up to 30% and robustness over 15 000 stretching cycles at 30% strain.

Textiles are considered to be particularly strong candidates for novel substrates in wearable electronics with high flexibility and stretchability. Due to their high surface-to-volume ratio, which enhances sensitivity, 1D organic semiconducting nanomaterials are more suitable for flexible and stretchable sensors than other film-type materials.^[282, 295] Oh et al. reported nanofiber-based phototransistors fabricated on PET/PDMS textile composite substrates.^[296] The organic nanofibers were obtained by electrospinning using a mixture of poly(3,3''-didodecylquarterthiophene) (PQT-12) and poly(ethylene oxide) (PEO). PDMS was used as both a buffer layer for flattening the PET textile and a dielectric layer. The PQT-12:PEO nanofiber OPTs showed a maximum responsivity of 930 mA/W under blue-light illumination. In addition, the OPTs exhibited highly stable device performance with an on-current retention of up to $82.3 \pm 6.7\%$ under a bending radius down to 0.75 mm and repeated tests over 1,000 cycles.

The magnitude of the photocurrent induced by illumination was found to be the result of two distinct factors: direct photocurrent related to electron-hole pair generation and current enhancement caused by a V_{th} shift.^[297] To achieve high sensitivity (light-to-dark current ratio), the gate voltage is set to approximately V_{th} to reduce the contribution of the field-effect current to the output current and enable extremely low dark current.^[212] Xu et.al report a flexible and electrolyte-gated-OPT device based on a highly transparent nanocomposite membrane involving a Ag NW network and iontronic material.^[234] The Ag NW network was directly embedded into an ionogel-type gate dielectric layer to serve as a flexible and transparent gate electrode, resulting in the formation of a nanometer-thick EDL at the

electrode-ionogel interface with an ultralarge interfacial capacitance of $\sim 2 \mu\text{F}/\text{cm}^2$ when not bent. In addition, the membrane when bent had a slightly smaller specific capacitance than that when not bent. By applying operational voltages close to $V_{\text{th}} = 1.5 \text{ V}$, high sensitivity of 7.5×10^5 and responsivity of $1.5 \times 10^3 \text{ A/W}$ can be obtained. Even when the bending radius was reduced to as small as 2 mm, the sensitivity remained at the level of 10^5 .

Organic photosensors for integrated pixels are particularly important for visible-imaging, nightvision, and motion detectors. Liu and co-workers^[294] reported a 470-nm-thick, integrated organic photosensor pixelated array consisting of three components: an organic light-dependent resistor (OLDR), an organic resistor (OR) as a load resistor, and an OFET as the readout element. As shown in Figure 12d-f, the 152-pixel detector array on polyacrylonitrile (PAN) foil was ultrathin and extremely light ($850 \text{ mg}/\text{m}^2$) and thus was operational under harsh bending conditions with a microscale radius of $5 \mu\text{m}$. In addition, the photosensor shows transconductance instead of conductance, thus giving a higher photo-to-dark on/off ratio of 10^8 . As a result, spatial mapping of the characteristics can be achieved by recording the current in each pixel with high accuracy under an intensity of $8.8 \text{ mW}/\text{cm}^2$ (Figure 12g). Later, in another report from the same group,^[288] they developed a filter-free and retina-inspired NIR flexible organic photosensor with N,N'-bis(2,6-diisopropylphenyl)-tetraphenoxy-3,4,9,10-perylenedicarboximide (ROT300), vanadyl phthalocyanine (VOPc) and N,N'-1H,1H-perfluorobutyldicyano-3,4,9,10-perylenedicarboximide (N1100) as the NIR photosensing element. In general, NIR organic photosensors require optical filters to reduce visible interference, thus making filter-free and anti-visible NIR imaging challenging. To solve this limitation, this organic retina system accommodated bimodal photoswitching and memory operations. The retina-like photosensor converted NIR (850 nm) signals into nonvolatile memory and acted as a dynamic photoswitch under green light (550 nm). In doing this, a filter-free but color-distinguishing photosensor is demonstrated. Then, 30 pixels were integrated and adhered to hemisphere surfaces. After exposure to a 1-s NIR pulse, reading of

the pixel currents clearly indicated the spatial location and NIR intensity supplied to the eye, which mimicked the imaging process of mammalian eyes.

4.3.3. Gas Sensor

Gas sensors have been widely reported for the detection a variety of hazardous gas leakages and emissions, such as nitrogen dioxide (NO_2 ^[298]), ammonia (NH_3 ^[233, 299]), hydrogen sulfide (H_2S ^[300]), phosphate vapors, hydrogen, etc. Wearable and portable gas sensors for the real-time monitoring of air quality and exhaled gas are regarded as economic and noninvasive technology for human health management and efficient disease detection.^[301] Compared to resistor-type sensors, OTFT-based sensors can efficiently translate the detected signals into changes in multiple transistor parameters, e.g., I_{DS} , μ and V_{th} . The response signals of these sensors can be easily amplified by applying a higher V_{GS} .^[302] The detection mechanism has been explained by the doping and trapping ability of the analyte towards the holes/electrons from the conduction channel and thus is closely related to both the semiconductor and the nature of the gate dielectric.^[303] Some crucial sensing performances, such as gas selectivity (specificity), sensitivity, LOD, and response/recovery time, are of more concern. So far, ppm (parts per million) and sub-ppm detection has been successfully realized with OTFTs.

Owing to their ordered crystal structures, which are optimal for achieving high surface areas and creating percolation pathways for gas,^[304] OTFTs employing small-molecule OSCs have been extensively investigated for highly sensitive gas sensors.^[305] The performance was strictly influenced by the morphology of the deposited organic film, grain boundaries, and traps. In general, bending strain can induce separation among small semiconductor molecules and increase the surface area of active layers, which facilitates gas molecules to interact directly.^[306] However, deformation also has a large influence on carrier transport in conductive channel. Therefore, maintaining percolation pathways without compromising charge carriers is essential for the realization of highly sensitive gas sensors.

For conjugated-polymer-based gas sensors, control of the film morphology and thickness, functionalization with chemical groups and the use of doped/blended conjugated-polymer composites as active layers have been widely investigated.^[307] To obtain high sensitivity, the thickness of the semiconducting layer should be downscaled since the sensing chemicals could reach the conductive channel faster by diffusion, which is distance dependent (**Figure 13a**).^[308, 309] However, achieving precise control of the conjugated-polymer thickness over a large area still remains a major limitation in solution-based manufacturing processes. Noh and co-workers reported a bar-coated ultrathin DPPT-TT film as the p-channel active layer for highly sensitive multigas sensors (Figure 13b). The gas sensitivity of the device with a film thickness less than 2 nm towards NH₃ was as high as 82%, while those for the 5.0 ± 0.5 nm and 12.8 ± 1.0 nm films were 27% and 10%. Gas pulses of NH₃ (10 ppm), ethanol (1,000 ppm) and even ethylene gas (1,000 ppm) were successfully detected by the 5- to 6-nm ultrathin film gas sensor, showing the response and recovery behavior (Figure 13c-e). In their further work, the same group reported a highly sensitive printed NH₃ OTFT gas sensor with ultrathin (<9 nm) fluorinated difluorobenzothiadiazole-dithienosilole polymer (PDFDT) as the active layer.^[299] These sensors detected NH₃ down to 1 ppm with high sensitivity (up to 56%) using bar-coated ultrathin (<4 nm) PDFDT layers without any receptor additives. This high performance is attributed to weak hydrogen bonds and electrostatic interactions between the fluorine atoms in PDFDT and hydrogen atoms in NH₃, demonstrating the advantages of molecularly designed polymers as channel materials.

Carbon nanotubes are also an ideal channel material for gas sensors, as their extremely high surface-to-volume ratio makes them highly sensitive to changes in the surrounding environment.^[310, 311] However, CNT-based gas sensors show a lack of selectivity and low recovery. Cui et al.^[298] used poly(9,9-dioctylfluorene) (PFO) derivative-sorted sc-SWCNTs as channel materials to construct NO₂ gas sensors. The use of high-purity semiconducting SWCNT networks over unsorted SWCNT networks was critical for obtaining high sensitivity

due to the high surface area and excellent conductivity. The printed OTFTs exhibited high on/off ratios of $\sim 10^6$ and a high mobility of up to $29.8 \text{ cm}^2/\text{Vs}$ at low operating voltage ($\pm 2 \text{ V}$). As a result, the NO_2 gas sensors showed good performance with a high sensitivity of $\sim 96\%$ and recovery time of 30 s when exposed to 60-ppm NO_2 at room temperature. To enhance their sensitivity, the CNTs could be functionalized with conducting polymers that can interact with the target molecules^[312] or metal nanoparticles to change the contacts resistance between the electrode material and the CNT channel.^[313]

The sensing performance of OTFT-based gas sensors can also be modulated by the source-drain electrode, dielectric layer, gate electrode, and even their interfaces. Taking the dielectric layer as an example, Katz et al. developed a self-healing polymer dielectric based on a blend of poly(2-hydroxypropylmethacrylate) (PHPMA)/(poly(ethyleneimine)) (PEI).^[233] This self-healing dielectric exhibited high effective capacitance of up to $1,400 \text{ nF/cm}^2$ at a thickness of 120 nm at $20\text{-}100 \text{ Hz}$. This highly polar self-healing dielectric layer had significant affinity towards NH_3 , resulting in more NH_3 being adsorbed at the interface between the dielectric layer and the semiconductor layer. Therefore, a P3HT-based gas sensor with this dielectric showed high sensitivity towards NH_3 with a LOD much lower than 0.5 ppm at a low operating voltage of -5 V . However, such polar dielectric layers have a detrimental effect on charge transport by acting as trap sites, which leads to low charge-carrier mobility and significant hysteresis.^[314] As high mobility directly determines the signal transfer speed, OTFT-based gas sensors with high gas capture ability must be developed without compromising their charge-carrier mobility.

4.3.4. Pressure Sensor

Flexible pressure sensors have potential applications in rollable touch displays, robotics and activity monitoring.^[315] Different applications require sensitivity at different pressure regimes; for example, sufficient sensitivity in medium-pressure regimes ($10\text{-}100 \text{ kPa}$) is suitable for

object manipulation, while that in low-pressure regimes (<10 kPa) is comparable to gentle touch.^[316] Most biomonitoring applications require high sensitivity in the low-pressure regime (<10 kPa), fast response time in the millisecond range, and low power consumption. Three kinds of transduction mechanisms that convert tactile stimuli into electrical signals exist: piezoresistivity,^[317, 318] capacitance,^[316] and piezoelectricity.^[319] Apart from utilizing a single OTFT as the pressure sensor, an integrated resistive-type pressure sensor or piezoelectric sensor with a transistor amplifier element can also be used to construct flexible pressure sensors with improved sensitivity.^[317, 318, 320]

For most OTFT-based pressure sensors, the pressure-sensitive element mainly depends on the capacitance change of the dielectric layer. Bao et al.^[321] presented flexible pressure-sensitive OTFTs by assembling separate layers *via* lamination, in which a large-area microstructured biocompatible elastomer PDMS layer acted as the dielectric layer (**Figure 14a**). Applied pressure induces a change in the capacitance of the compressible microstructured PDMS dielectric layer, which transduces as the I_{DS} current changes. They found that PDMS structures with pyramid-shaped features were more sensitive to pressure than line-shaped features,^[316, 317] and a larger spacing resulted in a higher normalized capacitance change and high sensitivity. The fabricated flexible pressure-sensitive sensor could be operated in the subthreshold regime, where the I_{DS} current was highly linearly dependent on the pressure-induced capacitance change. As a result, this pressure sensor showed a maximum sensitivity of 8.4 kPa^{-1} , a fast response time of < 10 ms, high stability over $> 15,000$ cycles and a low power consumption of < 1 mW. The flexible device could be operated with a bending radius down to 28 mm. Combining the high pressure sensitivity and fast response time, this flexible sensor could act as an electronic skin and be attached to a human wrist for noninvasive, high-fidelity, and continuous radial artery pulse wave monitoring (Figure 14b,c).

In addition to the dielectric layer, the introduction of an air gap is also useful for pressure-sensing applications. Di and co-workers^[322] reported flexible suspended gate OTFTs (SGOTFTs) to serve as versatile platforms for ultrasensitive pressure detectors. The unique device geometry allowed fine-tuning of the sensitivity and response range by adjusting the modulus and/or dimensions of the suspended gate. A flexible suspended gate with a low modulus was preferred to achieve ultrahigh sensitivity in the low-pressure regime. An unprecedented sensitivity of 192 kPa^{-1} , a low limit-of-detection pressure of $< 0.5 \text{ Pa}$ and a short response time of 10 ms were successfully realized. The device showed an ultralow power consumption of $< 100 \text{ nW}$ when operated under a battery voltage of 6 V . The outstanding sensing performance and good flexibility of SGOTFTs lead to many novel and fascinating applications, such as a wearable sensing array that was able to produce spatially resolved images with subtle imaging features (Figure 14d,e). When a laminated ultrathin Al foil (10 nm) was used as the suspended gate and the air gap was 4 mm , the sound signal response increased linearly from 0.05 to 0.3 Pa with a high sensitivity of 162.8 kPa^{-1} , thus allowing for the repeatable, real-time detection of different types of musical sounds (Figure 14f).

Most OTFT-based sensors are modulated by electrical signals, which lack active and direct interactions with the environment. In this regard, piezoelectric/tribotronic components are commonly used for transduction in self-powered pressure sensors.^[319, 320] Wang et al.^[323] developed a flexible organic tribotronic transistor (FOTT) for pressure and magnetic sensing. The fabricated FOTT had no top gate electrode and employed pentacene as the conductive channel and a PMMA/Cytop composite as the dielectric layer on a PET substrate. The I_{DS} can be greatly modulated by contact electrification between the dielectric layer and a $100\text{-}\mu\text{m}$ -thick fluorinated ethylene propylene (FEP) mobile triboelectric layer by applying an external pressure. With this principle, this FOTT can be further used as a pressure sensor that exhibits

a great sensitivity as high as $21\% \text{ Pa}^{-1}$ and fast response time of 110 ms in the pressure range of 20-1,000 Pa.

Previous work on stretchable pressure sensors required structural engineering to transfer the fabricated layers or whole devices onto pre-strained stretchable substrates. Complicated processes are used in these structural engineering methods, and the mechanical deformability of these devices is still limited to a small range of strain from 5% to 30% because of the inclusion of a non-stretchable OTFT channel. Lee and co-workers^[324] fabricated a stretchable sensor with both strain and temperature sensing by means of all-elastomeric transparent materials. A PEDOT:PSS/PU dispersion (PUD) composite elastomeric conductor was used as the electrode material, PU was used as the gate dielectric, reduced graphene oxide (rGO)/PU nanocomposite was used as the temperature-responsive channel layer, a Ag NWs/PEDOT:PSS/PUD composite was used as the strain-sensing layer, and PDMS was used as the substrate. This transparent and stretchable integrated platform can simultaneously monitor human skin temperature and muscle movement during human activities, such as drinking hot water. The development of flexible pressure sensors with improved sensitivity as well as accuracy and reliability is also important. This requires the sensor to measure only the normal pressure, even under extreme bending conditions. Someya et al.^[318] developed composite nanofibers composed of CNTs and graphene to reduce bending-induced interferences. Because of the nanoporous structure, the sensors exhibited an extremely small sensitivity to the bending-induced strain and maintained high sensitivity and excellent conformability down to a bending radius of $80 \mu\text{m}$.

In short, due to their perfect functionality of signal transduction and amplification, OTFTs provides an opportunity to reduce crosstalk between pixels with rapid addressing and low power consumption. The integration of flexible and stretchable multiple OTFT-based sensors into active OTFT arrays is crucial to realize large-area platforms for applications not only in

human-activity monitoring and personal healthcare^[325] but also in wearable military applications^[317] and human–machine interfaces.^[1, 326, 327]

4.4. Flexible Memory

The continuous monitoring of biological/physical signals requires a memory unit to store the recorded data. OTFT-based charge-trapping memory devices are emerging for solid-state data storage because of their downscaling ability, high data-storage density, fast switching speed, long-term reliability and overall integration compatibility with NAND and NOR architectures.^[328] By applying certain gate voltages, effective charge carriers can be injected from the OSCs to the charge-trapping layers *via* direct tunneling or Fowler–Nordheim tunneling.^[329] Depending on the charge-trapping materials, two main types of OTFT memory devices, namely, nano-floating-gate memory^[330, 331] and polymer electret memory,^[332] have received great research attention. To realize organic flexible nonvolatile memories, polymer electrets are promising components because of their simple and cost-effective solution processes on large-area substrates. More importantly, they can also retain stored information in the absence of power, even when the substrate is deformed by mechanical stress. The characteristics of polymer electrets, including π -conjugated side-chain moieties, dielectric constant, surface morphology and wettability, have been demonstrated for nonvolatile organic transistor memory devices.^[332, 333]

To fully integrate organic memories with wearable and flexible/stretchable electronic systems, it is important to develop a flexible memory device with a controllable operating regime. Chen et al.^[334] developed a series of polyimide (PI) electrets to investigate charge-transfer (CT) effects on the memory characteristics for n-channel flexible memories. The PITE(BMI-BMMD) electret with strong electron-donating ability enables the device to exhibit hole-trapping-only behavior, resulting in the inerasable write-one-read-many (WORM) type of memory. For D–A-type PI(APS-ODPA) and PI(APS-BPA) electrets, the derived memory devices exhibit programable flash-type characteristics. A flexible transistor

memory with multilevel data-storage behavior was demonstrated by using a PITE(BMI-BMMD) electret, which showed an excellent memory window and 10^5 -s retention stability even under a bent radius of 5 mm. Park et. al^[335] demonstrated an all-polymer flexible memory on a transparent 120- μ m-thick poly(ether sulfone) (PES) substrate with P(NDI2OD-T2) as the channel layer, PS as the tunneling layer, PVA as the charge-trapping layer and PMMA as the blocking layer (**Figure 15a**). After supplying $V_P/V_E = \pm 50$ V, the flexible memory device exhibited a memory window of approximately 15 V and memory current ratio of 10^4 . The reliability of the flexible device significantly depended upon the thickness of both the blocking and tunneling layers. Owing to the benefit of the all-polymer core structure, almost no change in V_{th} at the programmed and erased states was observed even after 1000 bending cycles under $r = 5.8$ mm (Figure 15b).

Although conventional metal nano-floating-gates (e.g., Au NPs and Ag NPs) have been widely investigated as charge-trapping elements in OTFT memories, they suffer from uncontrollable particle size and spacing due to the use of high-temperature thermal evaporation. Compared with metallic nano-floating-gates, flexible OTFT memory using semiconducting nano-floating-gates offers additional benefits such as facile control of charge trapping based on the molecular structure to realize functional memory properties^[340] and excellent processability to adapt them to large-area printing technology. To realize molecular floating gates, there are three main design strategies. The first strategy is to directly use solution-processed carbon materials (e.g., C60, SWNTs^[341]) as trapping sites. Zhou et.al^[342] reported tunable memory functions by employing a C60 molecular floating gate on a flexible PET substrate. The high mobility of C60 can help guide fast charge distribution and assist the charging process. The C60 floating gates showed ambipolar trapping behavior in air-stable p-type pentacene-based memories and unipolar trapping behavior in n-type copper hexadecafluorophthalocyanine (F₁₆CuPc)-based memories. The memory window was well-maintained even after 500 bending cycles both in tensile and compressive mode with a radius

of 10 mm. The second strategy is to utilize phase separation to form a floating gate with separated molecular microdomains.^[343, 344] Wang et al. used a blend solution consisting of PS and 6,13-bis(triisopropylsilylethynyl)pentacene (TIPS-Pen) to carry out this strategy. In the case of a low composition of TIPS-Pen, during the spin-coating process, TIPS-Pen aggregated and formed many separated microdomains, which were uniformly distributed in the insulating PS matrix as charge-trapping sites. The third strategy depends on the synergistic effect of blending a polymer electret and metal nanoparticles. Kim and co-workers^[336] reported a flexible P3HT-based memory using dual charge-trapping elements consisting of poly(2-vinyl naphthalene) (PVN) and Cu NPs on a PEN substrate. Under a bending radius of 3 mm, the flexible memory showed excellent reliability and reproducibility with a well-defined memory window over 30 V for more than 100 programming/erasing cycles (Figure 15c), which is attributed to the soft mechanical properties of P3HT and all charge-storage sites being surrounded by polymers.

Although research efforts have mainly focused on the development and engineering of charge-trapping materials, it is important to study organic semiconductors as well, as their properties are fundamentally related to operating speed, bias and reliability. Semiconducting ambipolar polymers have the intrinsic ability to transport electrons and holes, which provides an opportunity for the charge-trapping medium to efficiently trap both electrons and holes. Roy et al.^[345, 346] achieved a large memory window and distinct multilevel data storage by utilizing the ambipolar polymer poly(diketopyrrolopyrrololethiophenebenzothiadiazolethiophene) (PDPP-TBT). Functionalized rGO acted as the transparent charge-trapping layer, the work function of which could be tuned from 4.3 to 5.7 eV by an alkylsilane self-assembled monolayer (SAM). Interestingly, when considering the HOMO/LUMO level of PDPP-TBT, the tunable Fermi level of rGO induced a dramatic transition in the charging behavior from unipolar trapping of electrons to ambipolar trapping and eventually to unipolar trapping of holes. The as-fabricated flexible memory

transistor in both hole-enhancement and electron-enhancement mode did not exhibit obvious degradation in V_{th} after 500 bending cycles under a bending radius of 1 cm (both tensile and compressive strain of $\pm 1\%$). Nevertheless, the unbalanced ambipolarity of the OSCs caused an additional operating voltage. Additionally, strong ambipolar characteristics with equal hole and electron mobilities often lead to a decreased on/off current ratio due to the increased off current and short charge retention time. One structure that allows for extra tuning of memory functionality is that of heterostructure OTFTs utilizing both p-type and n-type materials as the active layers. Generally, OSC layers in this p-n heterostructure only function as charge-transport layers. Most recently, Yi et al.^[337] reported a flexible and 4-level nonvolatile OTFT memory based on pentacene/*N,N'*-ditridecylperylene-3,4,9,10-tetracarboxylic diimide (P13)/pentacene trilayer organic heterostructures on a PET substrate (Figure 15d). The discontinuous n-type P13 embedded in p-type pentacene layers provided not only electrons to the semiconductor layer to facilitate the electron-trapping process but also charge-trapping sites, which was attributed to the quantum well effect. This flexible memory showed a memory window over 30 V and on/off ratio of 10^2 . The variation in V_{th} in the programming/erasing state of the flexible memory is stable even after 10^4 bending cycles with a bending radius of 10 mm. These results provide a novel design strategy to take better advantage of OSC materials in OTFT memory.

Apart from the soft channel and charge-trapping materials, the mechanical deformation has immediate impact on the electrical performance of the device. Take pentacene as an example, the energy barrier for hole hopping decreases at compressive strain due to the smaller spacing between pentacene, while the tensile strain decreases the mobility because of the larger spacing.^[225] Ree et al reported bending stress could driven the phase transitions between the bulk phase and the thin-film phase in the pentacene film.^[347] Another reasonable explanation is that the effective thickness of the tunneling dielectric decreases under tensile strain and increases under compressive strain, which is induced by the Poisson effect (Figure

15e-g).^[348] As an example, Zhou et. al reported a pentacene-based flexible OTFT memory on a PET substrate,^[338] in which the reduced charge-tunneling barrier under tensile strain resulted in a negative shift in V_{th} , while the increased charge-tunneling barrier under compressive strain led to a positive shift in V_{th} . Therefore, the V_{th} of the memory transistor under tensile strain easily returns to the initial state after the erasing operation. As a result, the V_{th} of both the programmed and erased state could be modulated under certain strains.

Most reported OTFT memories are based on conventional planar architectures in which carriers are transported in the lateral direction, which is significantly inhibited by cracks or dislocations formed inside the channel under mechanical bending. To overcome this problem, an OTFT memory with vertical architecture was recently developed, which enables ultrashort channel length (nanoscale) and allows current to flow vertically across the semiconductor layer from the bottom source electrode to the top drain electrode.^[349] Chen et al. reported a vertical architecture flexible OTFT memory with the p-type semiconductor copolymer poly[2,5-bis(alkyl)pyrrolo[3,4-c]pyrrole-1,4(2H,5H)-dione-alt-5,5'-di(thiophen-2-yl)-2,2'-(E)-2-(2-(thiophen-2-yl)vinyl)-thiophene] (PDVT-8) and CdSe/ZnS QD trapping sites on a PI substrate (Figure 15h).^[339] As carrier transport was along the vertical direction, strain-induced in-plane cracks in the channel layer could be effectively eliminated compared with that in the planar architecture (Figure 15i,j). This flexible vertical memory device exhibited excellent mechanical stability with a memory ratio of more than 10^3 over 200 cycles with a bending radius of 10 mm. Moreover, the ultrashort channel length is simply determined by the thickness of the semiconductor layer (tens of nanometers), resulting in a fast operation speed down to 0.01 s.

5. Conclusions and Outlook

The continuous progress in organic materials and devices has greatly promoted the development flexible electronics. However, several challenges remain to be overcome. For

example, stretchability is still more challenging to achieve than simple flexibility.^[350] Structural engineering is an auxiliary method but usually requires complicated fabrication processes. One promising approach is based on the combination of employing flexible materials and structural engineering.

Moreover, the trade-off between mechanical and electrical characteristics is hard to balance. Although electrodes and substrates have already been engineered for good tolerance through rational structural design, the one-sided pursuit of high mechanical flexibility had led to extremely low device yields. Furthermore, the accurate and reliable performance evaluation of the device in dynamic mode remains difficult because the electrical properties vary significantly due to the strain induced by mechanical deformation.

Despite the significant advantages of solution-processing approaches, the stacking of all-flexible materials shows inherent limitations, such as the dissolution between neighboring layers, and the instability of organic materials (especially for n-type OSCs) under ambient and harsh environment. Understanding such instability mechanisms is a challenging but crucial task for commercialized application of organic flexible electronics. There is now various powerful technologies such as imaging (e.g., TEM, SEM), spectroscopy (e.g., XPS, Raman, EDS), topography (e.g., AFM, KPFM) and others, that are capable of probing the complex structure–property relationships. Currently, researchers should also examine the comprehensive use of flexible and highly stable components, such as hybrid electronics containing both organic and inorganic materials. The mutual penetration and mutual promotion between the two materials are becoming inevitable trends.

Additionally, the integration of multiple electronic functions to simultaneously check a variety of parameters in an ultrathin platform is crucial for the next generation of intelligent products. For a complete electronic system, essential functional requirements include power supply, signal transduction, signal amplification, signal filtering, signal transmission, signal reception and memory, resulting in two major problems. One is device miniaturization.

Moore's law can be specific for flexible devices, as the device is required to be thin enough (microscale) to work under a larger level of strain. The second problem is the compatibility of these devices in a system with different strain or non-uniform strain distribution. The solutions to the two problems are closely related to flexible circuit technology and rely on the joint efforts of chemists, physicists, biologists, materials scientists, and electrical engineers.

With the rapid development of novel organic materials, advanced fabrication techniques and rational geometric design strategies, we firmly believe that organic flexible electronics is bound to cause another revolution in human lifestyles in the next decade.

6. Acknowledgements

This work is financially supported by the Research Grants Council (RGC) of Hong Kong, China (Project No. C5015-15G) and the Hong Kong Polytechnic University (Project Nos. G-YBB7, G-SB51, G-YN09, 1-ZVGH, 1-ZVK1)

Received: ((will be filled in by the editorial staff))

Revised: ((will be filled in by the editorial staff))

Published online: ((will be filled in by the editorial staff))

References

- [1] B. C.-K. Tee, A. Chortos, A. Berndt, A. K. Nguyen, A. Tom, A. McGuire, Z. C. Lin, K. Tien, W.-G. Bae, H. Wang, P. Mei, H.-H. Chou, B. Cui, K. Deisseroth, T. N. Ng, Z. Bao, *Science* **2015**, *350*, 313.
- [2] K. Myny, *Nat. Electronics* **2018**, *1*, 30.
- [3] A. M. Hussain, M. M. Hussain, *Adv. Mater.* **2016**, *28*, 4219.
- [4] C. K. Chiang, C. R. Fincher, Y. W. Park, A. J. Heeger, H. Shirakawa, E. J. Louis, S. C. Gau, A. G. MacDiarmid, *Phys. Rev. Lett.* **1977**, *39*, 1098.
- [5] S. E. Root, S. Savagatrup, A. D. Printz, D. Rodriguez, D. J. Lipomi, *Chem. Rev.* **2017**, *117*, 6467.
- [6] K. Fukuda, T. Someya, *Adv. Mater.* **2017**, *29*, 1602736.
- [7] D. Li, W. Y. Lai, Y. Z. Zhang, W. Huang, *Adv. Mater.* **2018**, *30*, 1704738.
- [8] R. Xiong, A. M. Grant, R. Ma, S. Zhang, V. V. Tsukruk, *Mater. Sci. Eng., R* **2018**, *125*, 1.
- [9] M. Irimia-Vladu, *Chem. Soc. Rev.* **2014**, *43*, 588.
- [10] A. Chortos, J. Liu, Z. Bao, *Nat. Mater.* **2016**, *15*, 937.
- [11] T. Someya, Z. Bao, G. G. Malliaras, *Nature* **2016**, *540*, 379.
- [12] C. Wang, H. Dong, W. Hu, Y. Liu, D. Zhu, *Chem. Rev.* **2012**, *112*, 2208.
- [13] S. Choi, H. Lee, R. Ghaffari, T. Hyeon, D. H. Kim, *Adv. Mater.* **2016**, *28*, 4203.
- [14] Y. Yang, X. Yang, Y. Tan, Q. Yuan, *Nano Res.* **2017**, *10*, 1560.
- [15] L. Wang, D. Chen, K. Jiang, G. Shen, *Chem. Soc. Rev.* **2017**, *46*, 6764.
- [16] B. Zhu, H. Wang, W. R. Leow, Y. Cai, X. J. Loh, M. Y. Han, X. Chen, *Adv. Mater.* **2016**, *28*, 4250.
- [17] X. Chen, X. Han, Q. D. Shen, *Adv. Electron. Mater.* **2017**, *3*, 1600460.
- [18] J.-H. Bahk, H. Fang, K. Yazawa, A. Shakouri, *J. Mater. Chem. C* **2015**, *3*, 10362.
- [19] X. Bai, S. Lin, H. Wang, Y. Zong, H. Wang, Z. Huang, D. Li, C. Wang, H. Wu, *npj Flexible Electron.* **2018**, *2*, 3.
- [20] M.-G. Kang, H. Joon Park, S. Hyun Ahn, L. Jay Guo, *Sol. Energy Mater. Sol. Cells* **2010**, *94*, 1179.
- [21] X. Fan, N. X. Wang, J. Z. Wang, B. G. Xu, F. Yan, *Mater. Chem. Front.* **2018**, *2*, 355.
- [22] X. Fan, B. Xu, S. Liu, C. Cui, J. Wang, F. Yan, *ACS Appl. Mater. Interfaces* **2016**, *8*, 14029.
- [23] J. Y. Oh, S. Kim, H. K. Baik, U. Jeong, *Adv. Mater.* **2016**, *28*, 4455.
- [24] B. Yao, J. Zhang, T. Kou, Y. Song, T. Liu, Y. Li, *Adv. Sci.* **2017**, *4*, 1700107.
- [25] K. Rana, J. Singh, J.-H. Ahn, *J. Mater. Chem. C* **2014**, *2*, 2646.
- [26] J. Liu, C. S. Y. Tan, Z. Yu, N. Li, C. Abell, O. A. Scherman, *Adv. Mater.* **2017**, *29*, 1605325.
- [27] D. Chen, J. Liang, Q. Pei, *Sci. China: Chem.* **2016**, *59*, 659.
- [28] Y. Yu, C. Yan, Z. Zheng, *Adv. Mater.* **2014**, *26*, 5508.
- [29] S. Zhang, F. Cicoira, *Adv. Mater.* **2017**, *29*, 1703098.
- [30] Y. Sun, J. Lopez, H. W. Lee, N. Liu, G. Zheng, C. L. Wu, J. Sun, W. Liu, J. W. Chung, Z. Bao, Y. Cui, *Adv. Mater.* **2016**, *28*, 2455.
- [31] L. Huang, P. Jiang, D. Wang, Y. Luo, M. Li, H. Lee, R. A. Gerhardt, *Sens. Actuators, B* **2014**, *197*, 308.
- [32] E. K. Lee, M. Y. Lee, C. H. Park, H. R. Lee, J. H. Oh, *Adv. Mater.* **2017**, *29*, 1703638.
- [33] M. H. Park, J. Y. Kim, T. H. Han, T. S. Kim, H. Kim, T. W. Lee, *Adv. Mater.* **2015**, *27*, 4308.
- [34] J. Oh, J. H. Kim, S. Y. Lee, M. S. Kim, J. M. Kim, K. Park, Y. S. Kim, *IEEE Trans. Device Mater. Reliab.* **2018**, *18*, 1.

- [35] J. Nam, Y. Lee, W. Choi, C. S. Kim, H. Kim, J. Kim, D. H. Kim, S. Jo, *Adv. Energy Mater.* **2016**, *6*, 1601269.
- [36] S. P. Subbarao, M. E. Bahlke, I. Kymissis, *IEEE Trans. Electron Devices* **2010**, *57*, 153.
- [37] W. Tang, L. Feng, P. Yu, J. Zhao, X. Guo, *Adv. Electron. Mater.* **2016**, *2*, 1500454.
- [38] T. Cheng, Y. Zhang, W. Y. Lai, W. Huang, *Adv. Mater.* **2015**, *27*, 3349.
- [39] T. Q. Trung, N. E. Lee, *Adv. Mater.* **2017**, *29*, 1603167.
- [40] X. D. Chen, *Small Methods* **2017**, *1*, 1600029.
- [41] D.-H. Kim, J. Viventi, J. J. Amsden, J. Xiao, L. Vigeland, Y.-S. Kim, J. A. Blanco, B. Panilaitis, E. S. Frechette, D. Contreras, D. L. Kaplan, F. G. Omenetto, Y. Huang, K.-C. Hwang, M. R. Zakin, B. Litt, J. A. Rogers, *Nat. Mater.* **2010**, *9*, 511.
- [42] Z. Zhang, J. Du, D. Zhang, H. Sun, L. Yin, L. Ma, J. Chen, D. Ma, H.-M. Cheng, W. Ren, *Nat. Commun.* **2017**, *8*, 14560.
- [43] K. H. Ok, J. Kim, S. R. Park, Y. Kim, C. J. Lee, S. J. Hong, M. G. Kwak, N. Kim, C. J. Han, J. W. Kim, *Sci. Rep.* **2015**, *5*, 9464.
- [44] Q. Tai, F. Yan, *Adv. Mater.* **2017**, *29*, 1700192.
- [45] J. Y. Oh, S. Rondeau-Gagné, Y.-C. Chiu, A. Chortos, F. Lissel, G.-J. N. Wang, B. C. Schroeder, T. Kurosawa, J. Lopez, T. Katsumata, J. Xu, C. Zhu, X. Gu, W.-G. Bae, Y. Kim, L. Jin, J. W. Chung, J. B. H. Tok, Z. Bao, *Nature* **2016**, *539*, 411.
- [46] X. Pu, W. Hu, Z. L. Wang, *Small* **2018**, *14*, 1702817.
- [47] Y. Leterrier, in *Handbook of Flexible Organic Electronics: Materials, Manufacturing and Applications*, (Ed: S. Logothetidis), 2014, 3.
- [48] M. S. White, M. Kaltenbrunner, E. D. Głowacki, K. Gutnichenko, G. Kettlgruber, I. Graz, S. Aazou, C. Ulbricht, D. A. M. Egbe, M. C. Miron, Z. Major, M. C. Scharber, T. Sekitani, T. Someya, S. Bauer, N. S. Sariciftci, *Nat. Photonics* **2013**, *7*, 811.
- [49] D. M. Taylor, *Semicond. Sci. Technol.* **2015**, *30*, 054002.
- [50] D. Khim, H. Han, K. J. Baeg, J. Kim, S. W. Kwak, D. Y. Kim, Y. Y. Noh, *Adv. Mater.* **2013**, *25*, 4302.
- [51] L. Hu, H. S. Kim, J.-Y. Lee, P. Peumans, Y. Cui, *ACS Nano* **2010**, *4*, 2955.
- [52] D. Khim, G. S. Ryu, W. T. Park, H. Kim, M. Lee, Y. Y. Noh, *Adv. Mater.* **2016**, *28*, 2752.
- [53] A. Sandstrom, H. F. Dam, F. C. Krebs, L. Edman, *Nat. Commun.* **2012**, *3*, 1002.
- [54] K. K. Sears, M. Fievez, M. Gao, H. C. Weerasinghe, C. D. Easton, D. Vak, *Sol Rrl* **2017**, *1*, 1700059.
- [55] S. Das, B. Yang, G. Gu, P. C. Joshi, I. N. Ivanov, C. M. Rouleau, T. Aytug, D. B. Geohegan, K. Xiao, *ACS Photonics* **2015**, *2*, 680.
- [56] D. Y. Choi, H. W. Kang, H. J. Sung, S. S. Kim, *Nanoscale* **2013**, *5*, 977.
- [57] B. Roth, R. Søndergaard, F. Krebs, in *Handbook of Flexible Organic Electronics: Materials, Manufacturing and Applications*, (Ed: S. Logothetidis), Woodhead Publishing, 2014, 171.
- [58] H. Yang, W. R. Leow, X. Chen, *Small Methods* **2018**, *2*, 1700259.
- [59] M. Kim, H.-J. Ha, H.-J. Yun, I.-K. You, K.-J. Baeg, Y.-H. Kim, B.-K. Ju, *Org. Electron.* **2014**, *15*, 2677.
- [60] B. Roth, G. A. d. R. Benatto, M. Corazza, R. R. Søndergaard, S. A. Gevorgyan, M. Jørgensen, F. C. Krebs, *Adv. Energy Mater.* **2015**, *5*, 1401912.
- [61] J. Lee, A. R. Han, H. Yu, T. J. Shin, C. Yang, J. H. Oh, *J. Am. Chem. Soc.* **2013**, *135*, 9540.
- [62] S. Lee, H. Seong, S. G. Im, H. Moon, S. Yoo, *Nat. Commun.* **2017**, *8*, 725.
- [63] N. Chen, P. Kovacic, R. M. Howden, X. Wang, S. Lee, K. K. Gleason, *Adv. Energy Mater.* **2015**, *5*, 1401442.

- [64] S. M. Lee, J. H. Kwon, S. Kwon, K. C. Choi, *IEEE Trans. Electron Devices* **2017**, *64*, 1922.
- [65] Y. Im, S. Y. Byun, J. H. Kim, D. R. Lee, C. S. Oh, K. S. Yook, J. Y. Lee, *Adv. Funct. Mater.* **2017**, *27*.
- [66] Z. Yang, Z. Mao, Z. Xie, Y. Zhang, S. Liu, J. Zhao, J. Xu, Z. Chi, M. P. Aldred, *Chem. Soc. Rev.* **2017**, *46*, 915.
- [67] L. Duan, L. Hou, T.-W. Lee, J. Qiao, D. Zhang, G. Dong, L. Wang, Y. Qiu, *J. Mater. Chem.* **2010**, *20*, 6392.
- [68] H. Nakanotani, T. Higuchi, T. Furukawa, K. Masui, K. Morimoto, M. Numata, H. Tanaka, Y. Sagara, T. Yasuda, C. Adachi, *Nat. Commun.* **2014**, *5*, 4016.
- [69] L. Xiao, Y. Wu, J. Chen, Z. Yu, Y. Liu, J. Yao, H. Fu, *J. Phys. Chem. A* **2017**, *121*, 8652.
- [70] Q. Zhang, B. Li, S. Huang, H. Nomura, H. Tanaka, C. Adachi, *Nat. Photonics* **2014**, *8*, 326.
- [71] Y. Tao, K. Yuan, T. Chen, P. Xu, H. Li, R. Chen, C. Zheng, L. Zhang, W. Huang, *Adv. Mater.* **2014**, *26*, 7931.
- [72] K. S. Yook, J. Y. Lee, *Adv. Mater.* **2014**, *26*, 4218.
- [73] Y. Tao, C. Yang, J. Qin, *Chem. Soc. Rev.* **2011**, *40*, 2943.
- [74] G. M. Farinola, R. Ragni, *Chem. Soc. Rev.* **2011**, *40*, 3467.
- [75] J.-T. Chen, C.-S. Hsu, *Polymer* **2013**, *54*, 4045.
- [76] C. Sekine, Y. Tsubata, T. Yamada, M. Kitano, S. Doi, *Sci. Technol. Adv. Mater.* **2014**, *15*, 034203.
- [77] C.-R. Yin, S.-H. Ye, J. Zhao, M.-D. Yi, L.-H. Xie, Z.-Q. Lin, Y.-Z. Chang, F. Liu, H. Xu, N.-E. Shi, Y. Qian, W. Huang, *Macromolecules* **2011**, *44*, 4589.
- [78] F. So, D. Kondakov, *Adv. Mater.* **2010**, *22*, 3762.
- [79] A. Benor, S.-y. Takizawa, C. Pérez-Bolívar, P. Anzenbacher, *Org. Electron.* **2010**, *11*, 938.
- [80] I.-J. Park, T. I. Kim, T. Yoon, S. Kang, H. Cho, N. S. Cho, J.-I. Lee, T.-S. Kim, S.-Y. Choi, *Adv. Funct. Mater.* **2018**, *28*, 1704435.
- [81] X. Y. Zeng, Q. K. Zhang, R. M. Yu, C. Z. Lu, *Adv. Mater.* **2010**, *22*, 4484.
- [82] A. Kumar, C. Zhou, *ACS Nano* **2010**, *4*, 11.
- [83] W. Gaynor, S. Hofmann, M. G. Christoforo, C. Sachse, S. Mehra, A. Salleo, M. D. McGehee, M. C. Gather, B. Lussem, L. Muller-Meskamp, P. Peumans, K. Leo, *Adv. Mater.* **2013**, *25*, 4006.
- [84] E. Jung, C. Kim, M. Kim, H. Chae, J. H. Cho, S. M. Cho, *Org. Electron.* **2017**, *41*, 190.
- [85] J. Liang, L. Li, X. Niu, Z. Yu, Q. Pei, *Nat. Photonics* **2013**, *7*, 817.
- [86] Z. Yu, Q. Zhang, L. Li, Q. Chen, X. Niu, J. Liu, Q. Pei, *Adv. Mater.* **2011**, *23*, 664.
- [87] L. Li, J. Liang, S. Y. Chou, X. Zhu, X. Niu, ZhibinYu, Q. Pei, *Sci. Rep.* **2014**, *4*, 4307.
- [88] L. Li, Z. Yu, C. H. Chang, W. Hu, X. Niu, Q. Chen, Q. Pei, *Phys. Chem. Chem. Phys.* **2012**, *14*, 14249.
- [89] D. Yin, J. Feng, R. Ma, Y. F. Liu, Y. L. Zhang, X. L. Zhang, Y. G. Bi, Q. D. Chen, H. B. Sun, *Nat. Commun.* **2016**, *7*, 11573.
- [90] J. S. Lewis, M. S. Weaver, *IEEE J. Sel. Top. Quantum Electron.* **2004**, *10*, 45.
- [91] P. Jin-Seong, C. Heeyeop, C. Ho Kyoon, L. Sang In, *Semicond. Sci. Technol.* **2011**, *26*, 034001.
- [92] A. P. Ghosh, L. J. Gerenser, C. M. Jarman, J. E. Fornalik, *Appl. Phys. Lett.* **2005**, *86*, 223503.
- [93] H. Zhang, H. Ding, M. Wei, C. Li, B. Wei, J. Zhang, *Nanoscale Res. Lett.* **2015**, *10*, 169.

- [94] P. van de Weijer, P. C. P. Bouten, S. Unnikrishnan, H. B. Akkerman, J. J. Michels, T. M. B. van Mol, *Org. Electron.* **2017**, *44*, 94.
- [95] J. Fahlteich, C. Steiner, M. Top, D. Wynands, T. Wanski, S. Mogck, E. Kucukpinar, S. Amberg-Schwab, C. Boeffel, N. Schiller, *SID Symp. Dig. Tech. Pap.* **2015**, *46*, 106.
- [96] H. M. Etmimi, P. E. Mallon, R. D. Sanderson, *Eur. Polym. J.* **2013**, *49*, 3460.
- [97] T. Ming-Hung, Y. Hui-Huan, C. Kun-Yi, J. Jwo-Huei, L. Kung-Liang, W. Chin-Chiun, T. Feng-Yu, *Nanotechnology* **2016**, *27*, 295706.
- [98] Z. Wu, D. Ma, *Mater. Sci. Eng., R* **2016**, *107*, 1.
- [99] S.-H. Kim, M.-Y. Lee, K. Woo, H. Youn, T.-M. Lee, E. K. Lee, S. Kwon, *Int. J. Precis. Eng. Man.* **2017**, *18*, 1111.
- [100] F. Hermerschmidt, I. Burgues-Ceballos, A. Savva, E. D. Sepos, A. Lange, C. Boeffel, S. Nau, E. J. W. List-Kratochvil, S. A. Choulis, *Flexible Printed Electron.* **2016**, *1*, 035004.
- [101] L. Zhou, L. Yang, M. Yu, Y. Jiang, C. F. Liu, W. Y. Lai, W. Huang, *ACS Appl. Mater. Interfaces* **2017**, *9*, 40533.
- [102] J. B. Preinfalk, T. Eiselt, T. Wehlius, V. Rohnacher, T. Hanemann, G. Gomard, U. Lemmer, *ACS Photonics* **2017**, *4*, 928.
- [103] D. Han, Y. Khan, J. Ting, S. M. King, N. Yaacobi-Gross, M. J. Humphries, C. J. Newsome, A. C. Arias, *Adv. Mater.* **2017**, *29*, 1606206.
- [104] M. Vosgueritchian, J. B. H. Tok, Z. Bao, *Nat. Photonics* **2013**, *7*, 769.
- [105] T. Yokota, P. Zalar, M. Kaltenbrunner, H. Jinno, N. Matsuhisa, H. Kitanosako, Y. Tachibana, W. Yukita, M. Koizumi, T. Someya, *Sci. Adv.* **2016**, *2*, e1501856.
- [106] C. M. Lochner, Y. Khan, A. Pierre, A. C. Arias, *Nat. Commun.* **2014**, *5*, 5745.
- [107] J. T. Smith, B. Katchman, D. E. Kullman, U. Obahiagbon, Y.-K. Lee, B. O'Brien, G. B. Raupp, K. S. Anderson, J. Christen, *J. Disp. Technol.* **2016**, *12*, 273.
- [108] A. K. Bansal, S. Hou, O. Kulyk, E. M. Bowman, I. D. Samuel, *Adv. Mater.* **2015**, *27*, 7638.
- [109] M. Ramuz, B. C. Tee, J. B. Tok, Z. Bao, *Adv. Mater.* **2012**, *24*, 3223.
- [110] E. H. Kim, S. H. Cho, J. H. Lee, B. Jeong, R. H. Kim, S. Yu, T. W. Lee, W. Shim, C. Park, *Nat. Commun.* **2017**, *8*, 14964.
- [111] S. Y. Chou, R. Ma, Y. Li, F. Zhao, K. Tong, Z. Yu, Q. Pei, *ACS Nano* **2017**, *11*, 11368.
- [112] J. Liang, L. Li, K. Tong, Z. Ren, W. Hu, X. Niu, Y. Chen, Q. Pei, *ACS Nano* **2014**, *8*, 1590.
- [113] S. Liu, S. Lin, P. You, C. Surya, S. P. Lau, F. Yan, *Angew. Chem. Int. Ed.* **2017**, *129*, 13905.
- [114] S. Liu, R. Jiang, P. You, X. Zhu, J. Wang, F. Yan, *Energy Environ. Sci.* **2016**, *9*, 898.
- [115] S. Liu, P. You, J. Li, J. Li, C.-S. Lee, B. S. Ong, C. Surya, F. Yan, *Energy Environ. Sci.* **2015**, *8*, 1463.
- [116] S. Lin, S. Liu, Z. Yang, Y. Li, T. W. Ng, Z. Xu, Q. Bao, J. Hao, C.-S. Lee, C. Surya, F. Yan, S. P. Lau, *Adv. Funct. Mater.* **2016**, *26*, 864.
- [117] W. Zhao, S. Li, H. Yao, S. Zhang, Y. Zhang, B. Yang, J. Hou, *J. Am. Chem. Soc.* **2017**, *139*, 7148.
- [118] W. Zhao, D. Qian, S. Zhang, S. Li, O. Inganäs, F. Gao, J. Hou, *Adv. Mater.* **2016**, *28*, 4734.
- [119] G. Li, R. Zhu, Y. Yang, *Nat. Photonics* **2012**, *6*, 153.
- [120] J. You, L. Dou, K. Yoshimura, T. Kato, K. Ohya, T. Moriarty, K. Emery, C.-C. Chen, J. Gao, G. Li, Y. Yang, *Nat. Commun.* **2013**, *4*, 1446.
- [121] Z. Liu, J. Li, F. Yan, *Adv. Mater.* **2013**, *25*, 4296.
- [122] G. Yu, J. Gao, J. C. Hummelen, F. Wudl, A. J. Heeger, *Science* **1995**, *270*, 1789.
- [123] L. Dou, J. You, Z. Hong, Z. Xu, G. Li, R. A. Street, Y. Yang, *Adv. Mater.* **2013**, *25*, 6642.
- [124] Z. Liu, P. You, S. Liu, F. Yan, *ACS Nano* **2015**, *9*, 12026.

- [125] Z. Liu, J. Li, Z.-H. Sun, G. Tai, S.-P. Lau, F. Yan, *Acs Nano* **2011**, *6*, 810.
- [126] Z. Liu, S. P. Lau, F. Yan, *Chem. Soc. Rev.* **2015**, *44*, 5638.
- [127] Y. Li, *Acc. Chem. Res.* **2012**, *45*, 723.
- [128] L. Lu, T. Zheng, Q. Wu, A. M. Schneider, D. Zhao, L. Yu, *Chem. Rev.* **2015**, *115*, 12666.
- [129] X. Guo, A. Facchetti, T. J. Marks, *Chem. Rev.* **2014**, *114*, 8943.
- [130] P. Cheng, X. Zhan, *Chem. Soc. Rev.* **2016**, *45*, 2544.
- [131] J. C. Hummelen, B. W. Knight, F. LePeq, F. Wudl, J. Yao, C. L. Wilkins, *J. Org. Chem.* **1995**, *60*, 532.
- [132] S.-H. Lee, J.-H. Kim, T.-H. Shim, J.-G. Park, *Electron. Mater. Lett.* **2009**, *5*, 47.
- [133] S.-H. Lee, D.-H. Kim, J.-H. Kim, G.-S. Lee, J.-G. Park, *J. Phys. Chem. C* **2009**, *113*, 21915.
- [134] M. T. Dang, L. Hirsch, G. Wantz, *Adv. Mater.* **2011**, *23*, 3597.
- [135] T. Ameri, P. Khoram, J. Min, C. J. Brabec, *Adv. Mater.* **2013**, *25*, 4245.
- [136] Y. Liang, Y. Wu, D. Feng, S.-T. Tsai, H.-J. Son, G. Li, L. Yu, *J. Am. Chem. Soc.* **2009**, *131*, 56.
- [137] L. Lu, L. Yu, *Adv. Mater.* **2014**, *26*, 4413.
- [138] J. Hou, H.-Y. Chen, S. Zhang, R. I. Chen, Y. Yang, Y. Wu, G. Li, *J. Am. Chem. Soc.* **2009**, *131*, 15586.
- [139] H.-Y. Chen, J. Hou, S. Zhang, Y. Liang, G. Yang, Y. Yang, L. Yu, Y. Wu, G. Li, *Nat. Photonics* **2009**, *3*, 649.
- [140] L. Huo, S. Zhang, X. Guo, F. Xu, Y. Li, J. Hou, *Angew. Chem. Int. Ed.* **2011**, *50*, 9697.
- [141] S.-H. Liao, H.-J. Jhuo, Y.-S. Cheng, S.-A. Chen, *Adv. Mater.* **2013**, *25*, 4766.
- [142] S. Zhang, L. Ye, W. Zhao, D. Liu, H. Yao, J. Hou, *Macromolecules* **2014**, *47*, 4653.
- [143] P. Liu, K. Zhang, F. Liu, Y. Jin, S. Liu, T. P. Russell, H.-L. Yip, F. Huang, Y. Cao, *Chem. Mater.* **2014**, *26*, 3009.
- [144] L. Ye, S. Zhang, L. Huo, M. Zhang, J. Hou, *Acc. Chem. Res.* **2014**, *47*, 1595.
- [145] C. Cui, W.-Y. Wong, Y. Li, *Energy Environ. Sci.* **2014**, *7*, 2276.
- [146] W.-H. Chang, L. Meng, L. Dou, J. You, C.-C. Chen, Y. Yang, E. P. Young, G. Li, *Macromolecules* **2015**, *48*, 562.
- [147] Q. V. Hoang, C. E. Song, S.-J. Moon, S. K. Lee, J.-C. Lee, B. J. Kim, W. S. Shin, *Macromolecules* **2015**, *48*, 3918.
- [148] M. Qian, R. Zhang, J. Hao, W. Zhang, Q. Zhang, J. Wang, Y. Tao, S. Chen, J. Fang, W. Huang, *Adv. Mater.* **2015**, *27*, 3546.
- [149] A. a. F. Eftaiha, J.-P. Sun, I. G. Hill, G. C. Welch, *J. Mater. Chem. A* **2014**, *2*, 1201.
- [150] Y. Lin, X. Zhan, *Mate. Horiz.* **2014**, *1*, 470.
- [151] J. Roncali, P. Leriche, A. Cravino, *Adv. Mater.* **2007**, *19*, 2045.
- [152] H. Lin, S. Chen, Z. Li, J. Y. L. Lai, G. Yang, T. McAfee, K. Jiang, Y. Li, Y. Liu, H. Hu, J. Zhao, W. Ma, H. Ade, H. Yan, *Adv. Mater.* **2015**, *27*, 7299.
- [153] K. Liu, T. T. Larsen-Olsen, Y. Lin, M. Beliatas, E. Bundgaard, M. Jorgensen, F. C. Krebs, X. Zhan, *J. Mater. Chem. A* **2016**, *4*, 1044.
- [154] S. Oh, S. Badgajar, D. H. Kim, W.-E. Lee, N. Khan, M. Jahandar, S. Rasool, C. E. Song, H. K. Lee, W. S. Shin, J.-C. Lee, S.-J. Moon, S. K. Lee, *J. Mater. Chem. A* **2017**, *5*, 15923.
- [155] Y. Zang, C.-Z. Li, C.-C. Chueh, S. T. Williams, W. Jiang, Z.-H. Wang, J.-S. Yu, A. K. Y. Jen, *Adv. Mater.* **2014**, *26*, 5708.
- [156] Y. Zhong, M. T. Trinh, R. Chen, W. Wang, P. P. Khlyabich, B. Kumar, Q. Xu, C.-Y. Nam, M. Y. Sfeir, C. Black, M. L. Steigerwald, Y.-L. Loo, S. Xiao, F. Ng, X. Y. Zhu, C. Nuckolls, *J. Am. Chem. Soc.* **2014**, *136*, 15215.
- [157] Y. Liu, C. Mu, K. Jiang, J. Zhao, Y. Li, L. Zhang, Z. Li, J. Y. L. Lai, H. Hu, T. Ma, R. Hu, D. Yu, X. Huang, B. Z. Tang, H. Yan, *Adv. Mater.* **2015**, *27*, 1015.

- [158] K. Cnops, B. P. Rand, D. Cheyns, B. Verreert, M. A. Empl, P. Heremans, *Nat. Commun.* **2014**, *5*.
- [159] J. Zhao, Y. Li, H. Lin, Y. Liu, K. Jiang, C. Mu, T. Ma, J. Y. Lin Lai, H. Hu, D. Yu, H. Yan, *Energy Environ. Sci.* **2015**, *8*, 520.
- [160] Y. Lin, Q. He, F. Zhao, L. Huo, J. Mai, X. Lu, C.-J. Su, T. Li, J. Wang, J. Zhu, Y. Sun, C. Wang, X. Zhan, *J. Am. Chem. Soc.* **2016**, *138*, 2973.
- [161] X. Li, W. C. H. Choy, L. Huo, F. Xie, W. E. I. Sha, B. Ding, X. Guo, Y. Li, J. Hou, J. You, Y. Yang, *Adv. Mater.* **2012**, *24*, 3046.
- [162] C. E. Small, S. Chen, J. Subbiah, C. M. Amb, S.-W. Tsang, T.-H. Lai, J. R. Reynolds, F. So, *Nat. Photonics* **2012**, *6*, 115.
- [163] C. Cabanetos, A. El Labban, J. A. Bartelt, J. D. Douglas, W. R. Mateker, J. M. J. Fréchet, M. D. McGehee, P. M. Beaujuge, *J. Am. Chem. Soc.* **2013**, *135*, 4656.
- [164] T. Yang, M. Wang, C. Duan, X. Hu, L. Huang, J. Peng, F. Huang, X. Gong, *Energy Environ. Sci.* **2012**, *5*, 8208.
- [165] I. Osaka, T. Kakara, N. Takemura, T. Koganezawa, K. Takimiya, *J. Am. Chem. Soc.* **2013**, *135*, 8834.
- [166] J. You, C.-C. Chen, Z. Hong, K. Yoshimura, K. Ohya, R. Xu, S. Ye, J. Gao, G. Li, Y. Yang, *Adv. Mater.* **2013**, *25*, 3973.
- [167] H.-C. Chen, Y.-H. Chen, C.-C. Liu, Y.-C. Chien, S.-W. Chou, P.-T. Chou, *Chem. Mater.* **2012**, *24*, 4766.
- [168] K. Zhao, L. Ye, W. Zhao, S. Zhang, H. Yao, B. Xu, M. Sun, J. Hou, *J. Mater. Chem. C* **2015**, *3*, 9565.
- [169] J. Zhao, Y. Li, A. Hunt, J. Zhang, H. Yao, Z. Li, J. Zhang, F. Huang, H. Ade, H. Yan, *Adv. Mater.* **2016**, *28*, 1868.
- [170] Y. Liu, J. Zhao, Z. Li, C. Mu, W. Ma, H. Hu, K. Jiang, H. Lin, H. Ade, H. Yan, *Nat. Commun.* **2014**, *5*.
- [171] A. Facchetti, *Mater. Today* **2013**, *16*, 123.
- [172] T. Kim, J.-H. Kim, T. E. Kang, C. Lee, H. Kang, M. Shin, C. Wang, B. Ma, U. Jeong, T.-S. Kim, B. J. Kim, *Nat. Commun.* **2015**, *6*, 8547.
- [173] Y.-J. Hwang, B. A. E. Courtright, A. S. Ferreira, S. H. Tolbert, S. A. Jenekhe, *Adv. Mater.* **2015**, *27*, 4578.
- [174] L. Gao, Z.-G. Zhang, L. Xue, J. Min, J. Zhang, Z. Wei, Y. Li, *Adv. Mater.* **2016**, *28*, 1884.
- [175] D. Liu, T. L. Kelly, *Nat. Photonics* **2013**, *8*, 133.
- [176] J. You, Z. Hong, Y. Yang, Q. Chen, M. Cai, T.-B. Song, C.-C. Chen, S. Lu, Y. Liu, H. Zhou, Y. Yang, *ACS Nano* **2014**, *8*, 1674.
- [177] P. Docampo, J. M. Ball, M. Darwich, G. E. Eperon, H. J. Snaith, *Nat. Commun.* **2013**, *4*, 2761.
- [178] D. Yang, R. Yang, J. Zhang, Z. Yang, S. Liu, C. Li, *Energy Environ. Sci.* **2015**, *8*, 3208.
- [179] C. Roldan-Carmona, O. Malinkiewicz, A. Soriano, G. Minguez Espallargas, A. Garcia, P. Reinecke, T. Kroyer, M. I. Dar, M. K. Nazeeruddin, H. J. Bolink, *Energy Environ. Sci.* **2014**, *7*, 994.
- [180] X. Yin, P. Chen, M. Que, Y. Xing, W. Que, C. Niu, J. Shao, *ACS Nano* **2016**, *10*, 3630.
- [181] F. Di Giacomo, A. Fakharuddin, R. Jose, T. M. Brown, *Energy Environ. Sci.* **2016**, *9*, 3007.
- [182] Y. H. Kim, C. Sachse, M. L. Machala, C. May, L. Müller-Meskamp, K. Leo, *Adv. Funct. Mater.* **2011**, *21*, 1076.
- [183] B. Zhao, Z. He, X. Cheng, D. Qin, M. Yun, M. Wang, X. Huang, J. Wu, H. Wu, Y. Cao, *J. Mater. Chem. C* **2014**, *2*, 5077.
- [184] S.-I. Na, S.-S. Kim, J. Jo, D.-Y. Kim, *Adv. Mater.* **2008**, *20*, 4061.

- [185] A. M. Nardes, R. A. J. Janssen, M. Kemerink, *Adv. Funct. Mater.* **2008**, *18*, 865.
- [186] W. Zhang, B. Zhao, Z. He, X. Zhao, H. Wang, S. Yang, H. Wu, Y. Cao, *Energy Environ. Sci.* **2013**, *6*, 1956.
- [187] J. Huang, P. F. Miller, J. S. Wilson, A. J. de Mello, J. C. de Mello, D. D. C. Bradley, *Adv. Funct. Mater.* **2005**, *15*, 290.
- [188] E. Voroshazi, B. Verreet, A. Buri, R. Müller, D. Di Nuzzo, P. Heremans, *Org. Electron.* **2011**, *12*, 736.
- [189] V. Shrotriya, G. Li, Y. Yao, C.-W. Chu, Y. Yang, *Appl. Phys. Lett.* **2006**, *88*, 073508.
- [190] K. Kawano, R. Pacios, D. Poplavskyy, J. Nelson, D. D. C. Bradley, J. R. Durrant, *Sol. Energy Mater. Sol. Cells* **2006**, *90*, 3520.
- [191] L. Gomez De Arco, Y. Zhang, C. W. Schlenker, K. Ryu, M. E. Thompson, C. Zhou, *ACS Nano* **2010**, *4*, 2865.
- [192] Z. Yin, S. Sun, T. Salim, S. Wu, X. Huang, Q. He, Y. M. Lam, H. Zhang, *ACS Nano* **2010**, *4*, 5263.
- [193] I. Jeon, K. Cui, T. Chiba, A. Anisimov, A. G. Nasibulin, E. I. Kauppinen, S. Maruyama, Y. Matsuo, *J. Am. Chem. Soc.* **2015**, *137*, 7982.
- [194] Z. Liu, J. Li, Z.-H. Sun, G. Tai, S.-P. Lau, F. Yan, *ACS Nano* **2012**, *6*, 810.
- [195] L. Yang, T. Zhang, H. Zhou, S. C. Price, B. J. Wiley, W. You, *ACS Appl. Mater. Interfaces* **2011**, *3*, 4075.
- [196] C.-C. Chen, L. Dou, R. Zhu, C.-H. Chung, T.-B. Song, Y. B. Zheng, S. Hawks, G. Li, P. S. Weiss, Y. Yang, *ACS Nano* **2012**, *6*, 7185.
- [197] S. K. Hau, H.-L. Yip, N. S. Baek, J. Zou, K. O'Malley, A. K.-Y. Jen, *Appl. Phys. Lett.* **2008**, *92*, 253301.
- [198] J.-C. Wang, W.-T. Weng, M.-Y. Tsai, M.-K. Lee, S.-F. Horng, T.-P. Perng, C.-C. Kei, C.-C. Yu, H.-F. Meng, *J. Mater. Chem.* **2010**, *20*, 862.
- [199] M. Kaltenbrunner, M. S. White, E. D. Głowacki, T. Sekitani, T. Someya, N. S. Sariciftci, S. Bauer, *Nat. Commun.* **2012**, *3*, 770.
- [200] C.-Y. Chang, W.-K. Huang, Y.-C. Chang, K.-T. Lee, H.-Y. Siao, *Chem. Mater.* **2015**, *27*, 1869.
- [201] N. Kim, H. Kang, J.-H. Lee, S. Kee, S. H. Lee, K. Lee, *Adv. Mater.* **2015**, *27*, 2317.
- [202] M. W. Rowell, M. A. Topinka, M. D. McGehee, H.-J. Prall, G. Dennler, N. S. Sariciftci, L. Hu, G. Gruner, *Appl. Phys. Lett.* **2006**, *88*, 233506.
- [203] M. Song, D. S. You, K. Lim, S. Park, S. Jung, C. S. Kim, D.-H. Kim, D.-G. Kim, J.-K. Kim, J. Park, Y.-C. Kang, J. Heo, S.-H. Jin, J. H. Park, J.-W. Kang, *Adv. Funct. Mater.* **2013**, *23*, 4177.
- [204] J. H. Seo, I. Hwang, H.-D. Um, S. Lee, K. Lee, J. Park, H. Shin, T.-H. Kwon, S. J. Kang, K. Seo, *Adv. Mater.* **2017**, *29*, 1701479.
- [205] J. Huang, C.-Z. Li, C.-C. Chueh, S.-Q. Liu, J.-S. Yu, A. K. Y. Jen, *Adv. Energy Mater.* **2015**, *5*, 1500406.
- [206] X. Guo, Y. Xu, S. Ogier, T. N. Ng, M. Caironi, A. Perinot, L. Li, J. Zhao, W. Tang, R. A. Sporea, A. Nejim, J. Carrabina, P. Cain, F. Yan, *IEEE Trans. Electron Devices* **2017**, *64*, 1906.
- [207] Y. Yuan, G. Giri, A. L. Ayzner, A. P. Zoombelt, S. C. B. Mannsfeld, J. Chen, D. Nordlund, M. F. Toney, J. Huang, Z. Bao, *Nat. Commun.* **2014**, *5*, 3005.
- [208] W. Ou-Yang, T. Uemura, K. Miyake, S. Onish, T. Kato, M. Katayama, M. Kang, K. Takimiya, M. Ikeda, H. Kuwabara, M. Hamada, J. Takeya, *Appl. Phys. Lett.* **2012**, *101*, 223304.
- [209] X. Gao, Z. Zhao, *Adv. Energy Mater.* **2015**, *58*, 947.
- [210] Y. Kimura, T. Nagase, T. Kobayashi, A. Hamaguchi, Y. Ikeda, T. Shiro, K. Takimiya, H. Naito, *Adv. Mater.* **2015**, *27*, 727.

- [211] R. Hamilton, J. Smith, S. Ogier, M. Heeney, J. E. Anthony, I. McCulloch, J. Veres, D. D. C. Bradley, T. D. Anthopoulos, *Adv. Mater.* **2009**, *21*, 1166.
- [212] W.-Y. Chou, Y.-S. Lin, L.-L. Kuo, S.-J. Liu, H.-L. Cheng, F.-C. Tang, *J. Mater. Chem. C* **2014**, *2*, 626.
- [213] T. Lei, J.-Y. Wang, J. Pei, *Acc. Chem. Res.* **2014**, *47*, 1117.
- [214] S. Holliday, J. E. Donaghey, I. McCulloch, *Chem. Mater.* **2013**, *26*, 647.
- [215] Y. Zhao, Y. Guo, Y. Liu, *Adv. Mater.* **2013**, *25*, 5372.
- [216] X. Gao, Y. Hu, *J. Mater. Chem. C* **2014**, *2*, 3099.
- [217] H. Yan, Z. Chen, Y. Zheng, C. Newman, J. R. Quinn, F. Dotz, M. Kastler, A. Facchetti, *Nature* **2009**, *457*, 679.
- [218] K. J. Baeg, M. Caironi, Y. Y. Noh, *Adv. Mater.* **2013**, *25*, 4210.
- [219] Z. Chen, M. J. Lee, R. Shahid Ashraf, Y. Gu, S. Albert-Seifried, M. Meedom Nielsen, B. Schroeder, T. D. Anthopoulos, M. Heeney, I. McCulloch, H. Sirringhaus, *Adv. Mater.* **2012**, *24*, 647.
- [220] H. Luo, C. Yu, Z. Liu, G. Zhang, H. Geng, Y. Yi, K. Broch, Y. Hu, A. Sadhanala, L. Jiang, P. Qi, Z. Cai, H. Sirringhaus, D. Zhang, *Sci. Adv.* **2016**, *2*, e1600076.
- [221] M. Nikolka, I. Nasrallah, B. Rose, M. K. Ravva, K. Broch, A. Sadhanala, D. Harkin, J. Charmet, M. Hurhangee, A. Brown, S. Illig, P. Too, J. Jongman, I. McCulloch, J. L. Bredas, H. Sirringhaus, *Nat. Mater.* **2017**, *16*, 356.
- [222] Y. Liu, W. Hao, H. Yao, S. Li, Y. Wu, J. Zhu, L. Jiang, *Adv. Mater.* **2018**, *30*, 1705377.
- [223] H. H. Choi, K. Cho, C. D. Frisbie, H. Sirringhaus, V. Podzorov, *Nat. Mater.* **2017**, *17*, 2.
- [224] E. G. Bittle, J. I. Basham, T. N. Jackson, O. D. Jurchescu, D. J. Gundlach, *Nat. Commun.* **2016**, *7*, 10908.
- [225] A. N. Sokolov, Y. Cao, O. B. Johnson, Z. Bao, *Adv. Funct. Mater.* **2012**, *22*, 175.
- [226] R. P. Ortiz, A. Facchetti, T. J. Marks, *Chem. Rev.* **2010**, *110*, 205.
- [227] Y. Jiang, Y. Guo, Y. Liu, *Adv. Electron. Mater.* **2017**, *3*, 1700157.
- [228] J. Li, Z. Sun, F. Yan, *Adv. Mater.* **2012**, *24*, 88.
- [229] D. Liu, Q. Miao, *Mater. Chem. Front.* **2018**, *2*, 11.
- [230] G. Han, X. Wang, J. Zhang, G. Zhang, H. Yang, D. Hu, D. Sun, X. Wu, Y. Ye, H. Chen, T. Guo, *Org. Electron.* **2018**, *52*, 213.
- [231] C. Lu, W. Y. Lee, C. C. Shih, M. Y. Wen, W. C. Chen, *ACS Appl. Mater. Interfaces* **2017**, *9*, 25522.
- [232] Z. Liu, Z. Yin, S.-C. Chen, S. Dai, J. Huang, Q. Zheng, *Org. Electron.* **2018**, *53*, 205.
- [233] W. Huang, K. Besar, Y. Zhang, S. Yang, G. Wiedman, Y. Liu, W. Guo, J. Song, K. Hemker, K. Hristova, I. J. Kymissis, H. E. Katz, *Adv. Funct. Mater.* **2015**, *25*, 3745.
- [234] H. Xu, Q. Zhu, Y. Lv, K. Deng, Y. Deng, Q. Li, S. Qi, W. Chen, H. Zhang, *ACS Appl. Mater. Interfaces* **2017**, *9*, 18134.
- [235] T. Sekitani, T. Yokota, K. Kuribara, M. Kaltenbrunner, T. Fukushima, Y. Inoue, M. Sekino, T. Isoyama, Y. Abe, H. Onodera, T. Someya, *Nat. Commun.* **2016**, *7*, 11425.
- [236] Y. Yu, J. Zeng, C. Chen, Z. Xie, R. Guo, Z. Liu, X. Zhou, Y. Yang, Z. Zheng, *Adv. Mater.* **2014**, *26*, 810.
- [237] N. Matsuhisa, M. Kaltenbrunner, T. Yokota, H. Jinno, K. Kuribara, T. Sekitani, T. Someya, *Nat. Commun.* **2015**, *6*, 7461.
- [238] J. Huang, H. Zhu, Y. Chen, C. Preston, K. Rohrbach, J. Cumings, L. Hu, *ACS Nano* **2013**, *7*, 2106.
- [239] H. Sun, Y. Xu, Y.-Y. Noh, *IEEE Trans. Electron Devices* **2017**, *64*, 1944.
- [240] Y. Yoshimura, Y. Takeda, K. Fukuda, D. Kumaki, S. Tokito, *Org. Electron.* **2014**, *15*, 2696.
- [241] K. Fukuda, Y. Takeda, M. Mizukami, D. Kumaki, S. Tokito, *Sci. Rep.* **2014**, *4*, 3947.

- [242] J. F. Martinez Hardigree, H. E. Katz, *Acc. Chem. Res.* **2014**, *47*, 1369.
- [243] K. Finkensteller, *RFID handbook: fundamentals and applications in contactless smart cards, radio frequency identification and near-field communication*, John Wiley & Sons, 2010.
- [244] T.-H. Ke, R. Müller, B. Kam, M. Rockele, A. Chasin, K. Myny, S. Steudel, W. D. Oosterbaan, L. Lutsen, J. Genoe, L. van Leuken, B. van der Putten, P. Heremans, *Org. Electron.* **2014**, *15*, 1229.
- [245] K. Myny, S. Steudel, S. Smout, P. Vicca, F. Furthner, B. van der Putten, A. K. Tripathi, G. H. Gelinck, J. Genoe, W. Dehaene, *Org. Electron.* **2010**, *11*, 1176.
- [246] V. Fiore, P. Battiato, S. Abdinia, S. Jacobs, I. Chartier, R. Coppard, G. Klink, E. Cantatore, E. Ragonese, G. Palmisano, *IEEE T. Circuits-I.* **2015**, *62*, 1668.
- [247] S. Jacob, S. Abdinia, M. Benwadih, J. Bablet, I. Chartier, R. Gwoziecki, E. Cantatore, A. H. M. van Roermund, L. Maddiona, F. Tramontana, G. Maiellaro, L. Mariucci, M. Rapisarda, G. Palmisano, R. Coppard, *Solid State Electron.* **2013**, *84*, 167.
- [248] M. Jung, J. Kim, J. Noh, N. Lim, C. Lim, G. Lee, J. Kim, H. Kang, K. Jung, A. D. Leonard, J. M. Tour, G. Cho, *IEEE Trans. Electron Devices* **2010**, *57*, 571.
- [249] A. Falco, J. F. Salmeron, F. C. Loghin, P. Lugli, A. Rivadeneira, *Sensors* **2017**, *17*, 534.
- [250] M. Noda, N. Kobayashi, M. Katsuhara, A. Yumoto, S. Ushikura, R. Yasuda, N. Hirai, G. Yukawa, I. Yagi, K. Nomoto, T. Urabe, *J. Soc. Inf. Disp.* **2011**, *19*, 316.
- [251] J. Liang, L. Li, D. Chen, T. Hajagos, Z. Ren, S. Y. Chou, W. Hu, Q. Pei, *Nat. Commun.* **2015**, *6*, 7647.
- [252] T. Tsujimura, in *OLED Display Fundamentals and Applications*, John Wiley & Sons, Inc., 2017, 167.
- [253] M. Katsuhara, I. Yagi, A. Yumoto, M. Noda, N. Hirai, R. Yasuda, T. Moriwaki, S. Ushikura, A. Imaoka, T. Urabe, K. Nomoto, *J. Soc. Inf. Disp.* **2010**, *18*, 399.
- [254] H. Siringhaus, *Adv. Mater.* **2014**, *26*, 1319.
- [255] T. Q. Trung, N. E. Lee, *Adv. Mater.* **2016**, *28*, 4338.
- [256] S. T. Han, H. Peng, Q. Sun, S. Venkatesh, K. S. Chung, S. C. Lau, Y. Zhou, V. A. L. Roy, *Adv. Mater.* **2017**, *29*, 1700375.
- [257] Y. S. Rim, S. H. Bae, H. Chen, N. De Marco, Y. Yang, *Adv. Mater.* **2016**, *28*, 4415.
- [258] Y. Zang, D. Huang, C. A. Di, D. Zhu, *Adv. Mater.* **2016**, *28*, 4549.
- [259] Y. Fu, A. Yang, F. Yan, in *Seamless Healthcare Monitoring: Advancements in Wearable, Attachable, and Invisible Devices*, (Eds: T. Tamura, W. Chen), Springer International Publishing, Cham 2018, 335.
- [260] F. Yan, P. Estrela, Y. Mo, P. Migliorato, H. Maeda, S. Inoue, T. Shimoda, *Appl. Phys. Lett.* **2005**, *86*, 053901.
- [261] F. Torricelli, K. Manoli, E. Macchia, L. Torsi, M. Magliulo, in *Organic Sensors: Materials and Applications*, (Eds: E. Garcia-Breijó, B. G.-L. Perez, P. Cosseddu), Institution of Engineering and Technology, 2016, 71.
- [262] C. Liao, M. Zhang, M. Y. Yao, T. Hua, L. Li, F. Yan, *Adv. Mater.* **2015**, *27*, 7493.
- [263] Y.-Y. Lee, J.-H. Lee, J.-Y. Cho, N.-R. Kim, D.-H. Nam, I.-S. Choi, K. T. Nam, Y.-C. Joo, *Adv. Funct. Mater.* **2013**, *23*, 4020.
- [264] X. Fan, B. Xu, N. Wang, J. Wang, S. Liu, H. Wang, F. Yan, *Adv. Electron. Mater.* **2017**, *3*, 1600471.
- [265] S. Zhang, E. Hubis, C. Girard, P. Kumar, J. DeFranco, F. Cicoira, *J. Mater. Chem. C* **2016**, *4*, 1382.
- [266] S. Zhang, E. Hubis, G. Tomasello, G. Soliveri, P. Kumar, F. Cicoira, *Chem. Mater.* **2017**, *29*, 3126.
- [267] F. Cicoira, M. Sessolo, O. Yaghmazadeh, J. A. DeFranco, S. Y. Yang, G. G. Malliaras, *Adv. Mater.* **2010**, *22*, 1012.

- [268] L. Kergoat, B. Piro, D. T. Simon, M.-C. Pham, V. Nođ, M. Berggren, *Adv. Mater.* **2014**, *26*, 5658.
- [269] H. Tang, F. Yan, P. Lin, J. Xu, H. L. W. Chan, *Adv. Funct. Mater.* **2011**, *21*, 2264.
- [270] X. Guo, J. Liu, F. Liu, F. She, Q. Zheng, H. Tang, M. Ma, S. Yao, *Sens. Actuators, B* **2017**, *240*, 1075.
- [271] C. Liao, C. Mak, M. Zhang, H. L. Chan, F. Yan, *Adv. Mater.* **2015**, *27*, 676.
- [272] W. Lee, D. Kim, J. Rivnay, N. Matsuhisa, T. Lonjaret, T. Yokota, H. Yawo, M. Sekino, G. G. Malliaras, T. Someya, *Adv. Mater.* **2016**, *28*, 9722.
- [273] W. Lee, D. Kim, N. Matsuhisa, M. Nagase, M. Sekino, G. G. Malliaras, T. Yokota, T. Someya, *Proc. Natl. Acad. Sci. U.S.A.* **2017**, *114*, 10554.
- [274] R. X. He, P. Lin, Z. K. Liu, H. W. Zhu, X. Z. Zhao, H. L. W. Chan, F. Yan, *Nano Lett.* **2012**, *12*, 1404.
- [275] V. F. Curto, B. Marchiori, A. Hama, A.-M. Pappa, M. P. Ferro, M. Braendlein, J. Rivnay, M. Fioocchi, G. G. Malliaras, M. Ramuz, R. M. Owens, *Microsyst. Nanoeng.* **2017**, *3*, 17028.
- [276] P. Lin, X. Luo, I. M. Hsing, F. Yan, *Adv. Mater.* **2011**, *23*, 4035.
- [277] A. Campana, T. Cramer, D. T. Simon, M. Berggren, F. Biscarini, *Adv. Mater.* **2014**, *26*, 3874.
- [278] D. Khodagholy, J. Rivnay, M. Sessolo, M. Gurfinkel, P. Leleux, L. H. Jimison, E. Stavrinidou, T. Herve, S. Sanaur, R. M. Owens, G. G. Malliaras, *Nat. Commun.* **2013**, *4*, 2133.
- [279] C. Yao, Q. Li, J. Guo, F. Yan, I. M. Hsing, *Adv. Healthcare Mater.* **2015**, *4*, 528.
- [280] D. Khodagholy, T. Doublet, P. Quilichini, M. Gurfinkel, P. Leleux, A. Ghestem, E. Ismailova, T. Herve, S. Sanaur, C. Bernard, G. G. Malliaras, *Nat. Commun.* **2013**, *4*, 1575.
- [281] A. Williamson, M. Ferro, P. Leleux, E. Ismailova, A. Kaszas, T. Doublet, P. Quilichini, J. Rivnay, B. Rozsa, G. Katona, C. Bernard, G. G. Malliaras, *Adv. Mater.* **2015**, *27*, 4405.
- [282] C. Xie, F. Yan, *Small* **2017**, *13*, 1701822.
- [283] C. Xie, C. Mak, X. Tao, F. Yan, *Adv. Funct. Mater.* **2017**, *27*, 1603886.
- [284] K.-J. Baeg, M. Binda, D. Natali, M. Caironi, Y.-Y. Noh, *Adv. Mater.* **2013**, *25*, 4267.
- [285] H. Dong, H. Zhu, Q. Meng, X. Gong, W. Hu, *Chem. Soc. Rev.* **2012**, *41*, 1754.
- [286] T. Q. Trung, V. Q. Dang, H. B. Lee, D. I. Kim, S. Moon, N. E. Lee, H. Lee, *ACS Appl. Mater. Interfaces* **2017**, *9*, 35958.
- [287] Y. M. Song, Y. Xie, V. Malyarchuk, J. Xiao, I. Jung, K.-J. Choi, Z. Liu, H. Park, C. Lu, R.-H. Kim, R. Li, K. B. Crozier, Y. Huang, J. A. Rogers, *Nature* **2013**, *497*, 95.
- [288] H. Wang, H. Liu, Q. Zhao, Z. Ni, Y. Zou, J. Yang, L. Wang, Y. Sun, Y. Guo, W. Hu, Y. Liu, *Adv. Mater.* **2017**, *29*, 1701772.
- [289] J. A. Rogers, T. Someya, Y. Huang, *Science* **2010**, *327*, 1603.
- [290] S. Nam, J. Seo, H. Han, H. Kim, D. D. C. Bradley, Y. Kim, *ACS Appl. Mater. Interfaces* **2017**, *9*, 14983.
- [291] C. Xie, P. You, Z. K. Liu, L. Li, F. Yan, *Light: Sci. Appl.* **2017**, *6*, e17023.
- [292] J. Peng, Y. Chen, K. Zheng, T. Pullerits, Z. Liang, *Chem. Soc. Rev.* **2017**, *46*, 5714.
- [293] M. Ahmadi, T. Wu, B. Hu, *Adv. Mater.* **2017**, *29*, 1605242.
- [294] H. Wang, H. Liu, Q. Zhao, C. Cheng, W. Hu, Y. Liu, *Adv. Mater.* **2016**, *28*, 624.
- [295] H. Fang, W. Hu, *Adv. Sci.* **2017**, *4*, 1700323.
- [296] M. Y. Lee, J. Hong, E. K. Lee, H. Yu, H. Kim, J. U. Lee, W. Lee, J. H. Oh, *Adv. Funct. Mater.* **2016**, *26*, 1445.
- [297] R. Liguori, W. C. Sheets, A. Facchetti, A. Rubino, *Org. Electron.* **2016**, *28*, 147.
- [298] C. Zhou, J. Zhao, J. Ye, M. Tange, X. Zhang, W. Xu, K. Zhang, T. Okazaki, Z. Cui, *Carbon* **2016**, *108*, 372.
- [299] B. Nketia-Yawson, A. R. Jung, Y. Noh, G. S. Ryu, G. D. Tabi, K. K. Lee, B. Kim, Y. Y. Noh, *ACS Appl. Mater. Interfaces* **2017**, *9*, 7322.

- [300] C. Hua, Y. Shang, Y. Wang, J. Xu, Y. Zhang, X. Li, A. Cao, *Appl. Surf. Sci.* **2017**, *405*, 405.
- [301] T. Wang, Y. Guo, P. Wan, H. Zhang, X. Chen, X. Sun, *Small* **2016**, *12*, 3748.
- [302] X. G. Yu, N. J. Zhou, S. J. Han, H. Lin, D. B. Buchholz, J. S. Yu, R. P. H. Chang, T. J. Marks, A. Facchetti, *J. Mater. Chem. C* **2013**, *1*, 6532.
- [303] A.-M. Andringa, C. Piliago, I. Katsouras, P. W. M. Blom, D. M. d. Leeuw, *Chem. Mater.* **2013**, *26*, 773.
- [304] S. H. Yu, J. Cho, K. M. Sim, J. U. Ha, D. S. Chung, *ACS Appl. Mater. Interfaces* **2016**, *8*, 6570.
- [305] Y. Zang, F. Zhang, D. Huang, C. A. Di, Q. Meng, X. Gao, D. Zhu, *Adv. Mater.* **2014**, *26*, 2862.
- [306] M. Yi, Y. Guo, J. Guo, T. Yang, Y. Chai, Q. Fan, L. Xie, W. Huang, *J. Mater. Chem. C* **2014**, *2*, 2998.
- [307] B. Nketia-Yawson, Y.-Y. Noh, *Macromol. Res.* **2017**, *25*, 489.
- [308] F. Zhang, C. A. Di, N. Berdunov, Y. Hu, Y. Hu, X. Gao, Q. Meng, H. Sirringhaus, D. Zhu, *Adv. Mater.* **2013**, *25*, 1401.
- [309] L. Li, P. Gao, M. Baumgarten, K. Mullen, N. Lu, H. Fuchs, L. Chi, *Adv. Mater.* **2013**, *25*, 3419.
- [310] R. Md.Masud, I. D. Sh., M. A. M.R., J. S., T. Amanullah, *Sens. Rev.* **2017**, *37*, 127.
- [311] K. Chen, W. Gao, S. Emaminejad, D. Kiriya, H. Ota, H. Y. Nyein, K. Takei, A. Javey, *Adv. Mater.* **2016**, *28*, 4397.
- [312] A. S. Alshammari, M. R. Alenezi, K. T. Lai, S. R. P. Silva, *Mater. Lett.* **2017**, *189*, 299.
- [313] Y. Fang, M. Akbari, L. Sydanheimo, L. Ukkonen, M. M. Tentzeris, *Sci. Rep.* **2017**, *7*, 8988.
- [314] A. Klug, M. Denk, T. Bauer, M. Sandholzer, U. Scherf, C. Slugovc, E. J. W. List, *Org. Electron.* **2013**, *14*, 500.
- [315] Y. Zang, F. Zhang, C.-a. Di, D. Zhu, *Mater. Horiz.* **2015**, *2*, 140.
- [316] S. C. Mannsfeld, B. C. Tee, R. M. Stoltenberg, C. V. Chen, S. Barman, B. V. Muir, A. N. Sokolov, C. Reese, Z. Bao, *Nat. Mater.* **2010**, *9*, 859.
- [317] H. H. Chou, A. Nguyen, A. Chortos, J. W. To, C. Lu, J. Mei, T. Kurosawa, W. G. Bae, J. B. Tok, Z. Bao, *Nat. Commun.* **2015**, *6*, 8011.
- [318] S. Lee, A. Reuveny, J. Reeder, S. Lee, H. Jin, Q. Liu, T. Yokota, T. Sekitani, T. Isoyama, Y. Abe, Z. Suo, T. Someya, *Nat. Nanotechnol.* **2016**, *11*, 472.
- [319] L. Lin, Y. Xie, S. Wang, W. Wu, S. Niu, X. Wen, Z. L. Wang, *ACS Nano* **2013**, *7*, 8266.
- [320] T. Q. Trung, N. T. Tien, Y. G. Seol, N.-E. Lee, *Org. Electron.* **2012**, *13*, 533.
- [321] G. Schwartz, B. C. Tee, J. Mei, A. L. Appleton, D. H. Kim, H. Wang, Z. Bao, *Nat. Commun.* **2013**, *4*, 1859.
- [322] Y. Zang, F. Zhang, D. Huang, X. Gao, C. A. Di, D. Zhu, *Nat. Commun.* **2015**, *6*, 6269.
- [323] J. Zhao, H. Guo, Y. K. Pang, F. Xi, Z. W. Yang, G. Liu, T. Guo, G. Dong, C. Zhang, Z. L. Wang, *ACS Nano* **2017**, *11*, 11566.
- [324] T. Q. Trung, S. Ramasundaram, B. U. Hwang, N. E. Lee, *Adv. Mater.* **2016**, *28*, 502.
- [325] Y. Gao, H. Ota, E. W. Schaler, K. Chen, A. Zhao, W. Gao, H. M. Fahad, Y. Leng, A. Zheng, F. Xiong, C. Zhang, L. C. Tai, P. Zhao, R. S. Fearing, A. Javey, *Adv. Mater.* **2017**, *29*, 1701985.
- [326] C.-T. Chen, W.-Y. Lee, T.-L. Shen, H.-C. Wu, C.-C. Shih, B.-W. Ye, T.-Y. Lin, W.-C. Chen, Y.-F. Chen, *Adv. Electron. Mater.* **2017**, *3*, 1600548.
- [327] Y. Zang, H. Shen, D. Huang, C. A. Di, D. Zhu, *Adv. Mater.* **2017**, *29*, 1606088.
- [328] S. T. Han, Y. Zhou, V. A. Roy, *Adv. Mater.* **2013**, *25*, 5425.

- [329] H. Ling, W. Li, H. Li, M. Yi, L. Xie, L. Wang, Y. Ma, Y. Bao, F. Guo, W. Huang, *Org. Electron.* **2017**, *43*, 222.
- [330] C. C. Shih, W. Y. Lee, W. C. Chen, *Mater. Horiz.* **2016**, *3*, 294.
- [331] J. Li, F. Yan, *ACS Appl. Mater. Interfaces* **2014**, *6*, 12815.
- [332] Y.-H. Chou, H.-C. Chang, C.-L. Liu, W.-C. Chen, *Polym. Chem.* **2015**, *6*, 341.
- [333] H. Ling, J. Lin, M. Yi, B. Liu, W. Li, Z. Lin, L. Xie, Y. Bao, F. Guo, W. Huang, *ACS Appl. Mater. Interfaces* **2016**, *8*, 18969.
- [334] A. D. Yu, W. Y. Tung, Y. C. Chiu, C. C. Chueh, G. S. Liou, W. C. Chen, *Macromol. Rapid Commun.* **2014**, *35*, 1039.
- [335] W. Wang, S. K. Hwang, K. L. Kim, J. H. Lee, S. M. Cho, C. Park, *ACS Appl. Mater. Interfaces* **2015**, *7*, 10957.
- [336] M. Kang, D. Khim, W. T. Park, J. Kim, J. Kim, Y. Y. Noh, K. J. Baeg, D. Y. Kim, *Sci. Rep.* **2015**, *5*, 12299.
- [337] W. Li, F. Guo, H. Ling, P. Zhang, M. Yi, L. Wang, D. Wu, L. Xie, W. Huang, *Adv. Sci.* **2017**, *4*, 1700007.
- [338] Y. Zhou, S. T. Han, Z. X. Xu, V. A. Roy, *Nanoscale* **2013**, *5*, 1972.
- [339] D. Hu, X. Wang, H. Chen, T. Guo, *Adv. Funct. Mater.* **2017**, *27*, 1703541.
- [340] L. Zhang, T. Wu, Y. Guo, Y. Zhao, X. Sun, Y. Wen, G. Yu, Y. Liu, *Sci. Rep.* **2013**, *3*, 1080.
- [341] G. Wang, X. Liu, W. Wang, *IEEE Electron Device Lett.* **2018**, *39*, 111.
- [342] Y. Zhou, S. T. Han, Y. Yan, L. B. Huang, L. Zhou, J. Huang, V. A. Roy, *Sci. Rep.* **2013**, *3*, 3093.
- [343] C. Wu, W. Wang, J. Song, *IEEE Electron Device Lett.* **2017**, *38*, 641.
- [344] W. Wang, K. L. Kim, S. M. Cho, J. H. Lee, C. Park, *ACS Appl. Mater. Interfaces* **2016**, *8*, 33863.
- [345] Y. Zhou, S. T. Han, P. Sonar, V. A. Roy, *Sci. Rep.* **2013**, *3*, 2319.
- [346] S. T. Han, Y. Zhou, P. Sonar, H. Wei, L. Zhou, Y. Yan, C. S. Lee, V. A. Roy, *ACS Appl. Mater. Interfaces* **2015**, *7*, 1699.
- [347] C. Yang, J. Yoon, S. H. Kim, K. Hong, D. S. Chung, K. Heo, C. E. Park, M. Ree, *Appl. Phys. Lett.* **2008**, *92*, 243305.
- [348] T. Sekitani, Y. Kato, S. Iba, H. Shinaoka, T. Someya, T. Sakurai, S. Takagi, *Appl. Phys. Lett.* **2005**, *86*, 073511.
- [349] X. J. She, D. Gustafsson, H. Sirringhaus, *Adv. Mater.* **2017**, *29*, 1604769.
- [350] D. J. Lipomi, *Adv. Mater.* **2016**, *28*, 4180.

Figures:

Figure 1. Schematic illustration of four essential elements in the design and development of organic flexible electronics: material choice, architecture design, mechanical strain and processing technique.

Figure 2. a) The preparation of stretchable OLEDs: attaching the OLED/polymer film onto the prestretched elastomeric substrate, releasing the prestrains and obtaining OLEDs with ordered buckles. Photographs of the stretchable OLEDs based on a 200% prestrained substrate at 5 V with strain values of b) 0%, c) 40%, d) 80%, e) 100%, f) mounted on an extended bent finger joint with 55–60% strain. g) Normalized luminance and current efficiency as a function of the number of stretch-release cycles for the stretchable OLEDs at 5 V between 0% and 40% strain. Reproduced with permission.^[89] Copyright 2016, Springer Nature.

Figure 3. a) Schematic diagram of the ultraflexible PLED. b) Photograph of the ultraflexible green PLED that was crumpled. c) Photograph of a red seven-segment PLEDs displayed on hand. d) Cyclic stretching test of the green PLED. After 1000 stretching cycle tests, the light intensity was decreased by only 10%. e) Operation principle of the reflective pulse oximeter consisting a red PLED, a green PLED and an OPD. f) Long-term measurement of the pulse wave using a red PLED and OPD. g) Output signal from OPD with 99% oxygenation of blood. The green and red lines represent the signals when the green and red PLEDs, respectively, were operated. Reproduced with permission.^[105] Copyright 2016, AAAS.

Figure 4. a) HOMO/LUMO energy levels and b) Optical absorption spectra of PNDIS-HD and PBDTT-FTTE polymers. a,b) Reproduced with permission.^[173] Copyright 2015, John Wiley & Sons. c) Device structure of the all polymer solar cell, d) Absorption spectra of J51 film, N2200 films and their polymer blend film. c,d) Reproduced with permission.^[174] Copyright 2017, John Wiley & Sons.

Figure 5. Sub-2- μm -thick OPVs. a) Scheme of the ultra-light and flexible OPV. Scale bar: (also in b, c) 2 mm. b) Stretchable solar cells, flat (left), at 30% (middle) and 50% (right) quasi-linear compression. c) The device attached to the elastomeric support, under three-dimensional deformation by pressure from a plastic tube. d) SEM image of the PET surface of the solar cell in compressed state. Scale bar: 500 μm . e) The I - V curves are shown at 1 (black), 11 (red) and 22 (blue) cycles for both the fully extended and 50% (quasi-linear) compressed states. f) Device performance metrics plotted at each of the 22 cycles for the fully extended state. Green downward triangles represent FF, blue upward triangles V_{oc} , red circles I_{sc} and black diamonds power. Reproduced with permission.^[199] Copyright 2012, Springer Nature.

Figure 6. a) The optical transmittance of the PET/ITO and glass/ITO substrate, b) The J - V characteristics of the flexible OPVs, c) Certified J - V curves of the flexible PTB7:PC₇₁BM solar cells with a PCE of 8.709%. a-c) Reproduced with permission.^[183] Copyright 2014, Royal Society of Chemistry. d) Schematic of the device architecture of the double-junction tandem solar cell, e) J - V curves of the double-junction tandem solar cells (100 mW/cm² light intensity: G-glass substrate, H-PEN substrate; 10 mW/cm² light intensity: I-glass substrate, J-PEN substrate), f) a typical photograph of a flexible device with PCE of 9.2%. d-f) Reproduced with permission.^[200] Copyright 2015, American Chemical Society.

Figure 7. a) J - V and b) EQE curves for the PBDTTTPD:PCBM-based OPV and the all-polymer OPV based on PBDTTTPD:P(NDI2HD-T). Normalized conductance of PBDTTTPD:PCBM and PBDTTTPD:P(NDI2HD-T) blend films c) after bending at various r values and d) after multiple cycles of bending at $r=1.5$ mm. SEM images of e) PBDTTTPD:PCBM and f) PBDTTTPD:P(NDI2HD-T) blend films after bending at $r=1.0$ mm. The scale bars are 500 nm. Reproduced with permission.^[172] Copyright 2015, Springer Nature.

Figure 8. a) UV-Vis transmittance spectra of graphene films with 1 to 4 layers. b) J - V characteristics of OPVs with different numbers of layers of graphene anode doped with PEDOT:PSS and Au NPs or PEDOT:PSS only. c) Bending performance of a flexible OPV with graphene anode. Inset: the schematic of a flexible OPV with an inverted structure of PI/Ag/ZnO/P3HT:PCBM/PEDOT:PSS/Graphene/PMMA. d) Evolution of PCEs of package-free OPVs with 1 to 4 layers of graphene or Au top electrodes measured in air. Reproduced with permission.^[121] Copyright 2013, John Wiley & Sons.

Figure 9. a) The J - V curves and b) EQE spectra of OPVs used different flexible transparent electrodes and substrates, Inset: a photo of a flexible OPV. a,b) Reproduced with permission.^[204] Copyright 2017, John Wiley & Sons. c) OPV device architecture with semitransparent top grids and UTMF electrode, d) J - V characteristics of ITO-based device and the microcavity device on glass and PET substrates. Reproduced with permission.^[205] Copyright 2015, John Wiley & Sons.

Figure 10. a) Optical image of the all-printed and roll-to-roll-printable 13.56-MHz-operated 1-bit RFID tag on plastic foils. Reproduced with permission.^[249] Copyright 2017, MDPI. b) Photographs of the rollable OTFT-driven OLED display with $r = 4$ mm. Reproduced with permission.^[250] Copyright 2011, John Wiley & Sons. The OLED controlled by a stretchable SWCNT-AgNW TFT under 30% strain: c) Output ($I_{\text{OLED}}-V_{\text{DD}}$) characteristics, d) Transfer ($I_{\text{OLED}}-V_{\text{GS}}$) characteristics. The inset photographs show the OLED brightness under 30% strain. c,d) Reproduced with permission.^[251] Copyright 2015, Springer Nature.

Figure 11. a) Photographs for flexible OECTs attached on different surfaces. b) The transfer characteristics of the flexible OECT measured in PBS solution after the bending tests up to 1000 times. $V_{\text{DS}} = 0.05$ V. c) Channel current responses of the flexible OECT as a glucose sensor for Saliva Testing. Inset: transfer characteristic of the OECT measured in PBS solution. a,b,c) Reproduced with permission.^[271] Copyright 2015, John Wiley & Sons. d) Photograph of a 2×2 electrophysiology array on muscle tissue (Scale bar; 2 mm). e) The spatial distribution of the myoelectric signal intensity measured by a 2×2 electrophysiology array. d,e) Reproduced with permission.^[272] Copyright 2016, John Wiley & Sons. f) The spatial

distribution of the brain signal intensity measured by a 3×5 transparent electrophysiology array. The electric potential was calculated using each OECT's transconductance. Reproduced with permission.^[273] Copyright 2017, National Academy of Sciences.

Figure 12. a) Photograph of the flexible $\text{CH}_3\text{NH}_3\text{PbI}_{3-x}\text{Cl}_x/\text{PEDOT:PSS}$ phototransistor. b) Responsivity of the flexible phototransistor before (solid dots) and after (hollow dots) a bending test. c) Time-dependent photoresponse of the device to periodic on/off illumination before and after the bending test. Light wavelength: 895 nm. a,b,c) Reproduced with permission.^[291] Copyright 2017, Springer Nature. Photographs for a $3.6 \times 3.6 \text{ cm}^2$ array d) conformed to a human hand. Scale bar, 2.4 cm. e) formed intimate contact with loops and whorls on the human finger. Scale bar, 1 cm. f) transferred on a silver grid (a diameter of 200 μm). Scale bar, 1 cm. g) A spatial mapping of the Chinese characters "乙未" using the 152 pixel array. d,e,f,g) Reproduced with permission.^[294] Copyright 2016, John Wiley & Sons.

Figure 13. a) Illustration of a gas sensor based on a thin or thick semiconducting film. b) Schematic illustration of the bar-coating process (inset: interface at solution and wire-wound bar). c) The corresponding response curves of the DPPT-TT with 5–6 nm device exposure to c) ammonia (10 ppm), d) ethanol (1,000 ppm), and e) ethylene (1,000 ppm) gas pulse. Pink or blue dots referring to $V_{\text{DS}} = -20\text{V}$ and -5V , respectively. Reproduced with permission.^[52] Copyright 2016, John Wiley & Sons.

Figure 14. a) SEM pictures (scale bar, 10 μm) of microstructured PDMS: pyramids with 3 mm height and spacing of 8.85 mm, taken at 45 tilt angle. b) Photographs for the flexible pressure sensor attached to the wrist to test the pulse wave of the radial artery. c) Averaged signal from 16 periods (separate measurements). a,b,c) Reproduced with permission.^[321] Copyright 2013, Springer Nature. d) A photograph and (e) resulting current mapping of a flexible 8×8 pressure-sensing array to the subtle touches, the array with a total area of $6 \times 6 \text{ cm}^2$ and each pixel has an area of $\sim 2.5 \text{ mm}^2$; scale bar, 5 cm. f) Electric signal response of a sensor to the same music for two times. d,e,f) Reproduced with permission.^[322] Copyright 2015, Springer Nature.

Figure 15. a) Schematic configuration of arrays of flexible OTFT memory on a PES substrate. b) The programmed and erased V_{th} of the flexible memory at the flat condition after selected tensile and compressive bending cycles. a,b) Reproduced with permission.^[335] Copyright 2015, American Chemical Society. c) V_{th} shifts of the flexible synergistic memory device after programming and erasing at different bending radii (inset: photograph of the flexible memory device). Reproduced with permission.^[336] Copyright 2015, Springer Nature. d) Variation in V_{th} at the programming/erasing state as a function of mechanical bending cycles with a bending radius of 10 mm. (inset) A photograph of flexible memory device array under mechanical bending. Reproduced with permission.^[337] Copyright 2017, John Wiley & Sons. Schematic illustrations of the memory arrays at e) zero strain, f) tensile strain and g) compressive strain. e,f,g) Reproduced with permission.^[338] Copyright 2013, Royal Society of Chemistry. h) Schematic diagram of the device architecture of flexible vertical memory.

Schematic illustration of the current transport in i) conventional planar memory and j) vertical memory on flexible PI substrate. The arrows represent the current flow direction. h,i,j) Reproduced with permission.^[339] Copyright 2017, John Wiley & Sons.

Table 1. Summary of flexible OLEDs for display, lightning and sensing applications.

Application	Substrate (Transparent Anode)	Organic Emitter	Performance		Ref.
			Flexibility ^{a)}	Electronic Functionality ^{b)}	
Lightning	PET (GO-AgNW/PUA)	White emitting polymer+OXD-7	survive after 100 stretching cycles between 0 and 40% strain and can be stretched up to 130% linear strain at room temperature	CIE close to pure white, 1.5 cd/A at 280 cd/m ² for a fresh PLED, maximum 4.0 cd/A	[112]
Display	PET foil (PEDOT:PSS)	AnE-PV <i>stat</i>	2 μ m thick, bending radii under 10 μ m, cyclic tensile strains up to 100%	Red and orange luminance greater than 100 cd/m ² .	[48]
Display	PUA matrix (AgNW-PUA)	SuperYellow+ ETPTA+PEO+ LiTf	strains of up to 120%	a maximum brightness of 2,200 cd/m ² and an efficiency of 11 cd/A (emission from both sides), 5 \times 5 pixel array	[85]
Pulse oximeter	Parylene (ITO)	Blue (fluorescent emitters), green and red (phosphorescent emitters)	3 μ m thick, bending radii under 100 μ m, repeatedly sustain up to 60% compression	EQE >6.2% 10 mA/cm ² for RGB, PPG signal with amplitudes of 100 to 200 mV	[105]
Pulse oximeter	PEN (ITO)	F8BT+ TFB+TBT	Placed on the wrist	signal magnitude with total flux. 1.1, 1.0, and 1.2 mV PPG signals are obtained using 0.68, 0.89, and 0.19 mW of fluxes, for green, red, and NIR PLEDs.	[103]
Interactive displays	PET (in-plane ITO)	Super Yellow+MWNTs	Several hundred cd/m ² maintained at a bending radius of 0.5 mm, 1,000 bending cycles	luminance of 2,000 cd/m ² and a response time of 100 ms at 30 V and 100 kHz for fingerprint detection and imaging.	[110]
Touch- responsive	PET (ITO/AgNW-PU)	MAPbBr ₃ +PEO	68% transparency, 6 mm bending radius	the minimum pressure of 0.55 MPa, 1030 cd/m ² at 6 V, repeated pressure- luminance of 1,100 cycles under 1.67 Hz	[111]

^{a)} Referring to the bending radii, bending cycles, strains, transparency, etc; ^{b)} Including emitting and other electronic functions, such as sensing.

Table 2. Summary of the performance of state-of-the-art binary blend BHJ OPVs.

Polymer	Polymer:PC ₇₁ BM Ratio	J_{sc} [mA/cm ²]	V_{oc} [V]	FF [%]	η [%]	Ref.
PBDTTT-C-T	1:1.5	18.4	0.76	63	8.8	[161]
PDTG-TPD	1:1.5	14.0	0.86	67	8.5	[162]
PBDTTPD	1:1.5	12.6	0.97	70	8.5	[163]
PBDT-DTNT	1:1.5	17.4	0.75	61	8.4	[164]
PNNT-12HD	1:2	15.6	0.82	64	8.2	[165]
PDTP-DFBT	1:2	18.6	0.69	63	8.1	[166]
PBDT-TFQ	1:1	17.9	0.76	58	8.0	[167]
PBDT-TS1	1:1.5	17.5	0.80	68	9.5	[168]
PTB7-Th	1:1.5	16.9	0.78	68	9.0	[142]
PfBX4T-2DT	1:1.2	15.8	0.88	66	9.1	[169]
PfBT4T-2OD	1:1.2	18.4	0.77	0.74	10.5	[170]

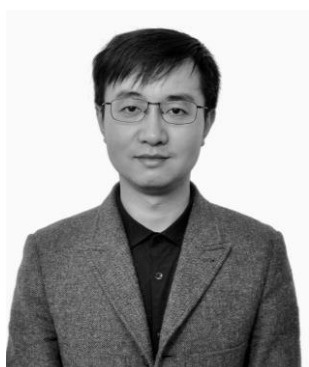
Table 3. Summary of flexible OTFTs for sensing applications.

Sensor types	Substrate (Dielectric)	Active organic material	Performance		Ref.
			Flexibility ^{a)}	Sensing	
Bio ^{b)}	PET	PEDOT:PSS	Outcurve/incurve bending up to 5% strain	DNA (LOD 10 pM)	[276]
Bio	PET	PEDOT:PSS	1,000 bending cycles	uric acid (LOD 10 nM)	[271]
Bio	parylene	PEDOT:PSS	2 μm thick, unchanged transconductance when crumpled	a 4 mm ² spatial resolution and a 3 kHz temporal resolution in measuring myoelectric signal	[272]
Light	PET/PDMS textile composite	PQT-12	on-current retention up to 82.3 (\pm 6.7) % under bending radius 0.75 mm and 1,000 cycles	$R=930$ mA/W under blue light, EQE=246%	[296]
Light	PAN foil (PPO)	Pentacene (channel) PDI-C8/ Pc (resistor)	470 nm thick, 850 mg/m ² , Loss of 9% photocurrents bending at 5 μm	high on/off ratio of 10 ⁸ , amplification of optical signals by over 10 ⁴ times	[294]
Light	PAN foil (P(VDFTRFE-CFE))	PIID-TT (channel) ROT300/VOPc/N1100 (photosensing element)	sensor array operational on hemisphere surface	62 dB NIR-to-memory, 86 dB green light detection at nW reading power	[288]
Gas	AryLite polyester (PMMA)	TIPS-pentacene	highly transparent (>80%), bending radius ~2.5 mm	multiple OTFT parameter changes ranging from 0 to 100 ppm to NH ₃	[302]
Gas	PET (PAN+PMSQ)	NDI(2OD)(4tBuPh)-DTYM2	4 nm transparent and ultrathin sensor	10 ppm NH ₃ with a response and recovery time of less than 20 seconds	[308]
Gas	PET (PHPMA+PEI)	P3HT/5FPE-NTCDI	0.5 MPa at a strain of 300 % self-healing	0.5 ppm to NH ₃	[233]
Pressure	Au-coated PET (parylene)	DNTT	2 μm thick, bending-insensitive down to 80 μm and optically transparent	~0.6–1.5 kPa under complex bending and wrinkling, response time of ~20 and 5 ms	[318]
Pressure	PI/PET (CYTOP/PMMA/PS)	PDPP3T\ NDI3HU-DTYM2	bending radii of 0.25 mm	ultra-high sensitivity of 192 kPa ⁻¹ , a fast response time of <10 ms and a low power consumption of <100 nW	[322]
Pressure	PI (PDMS)	PII2T-Si	operate the device at all bending radii down to 28 mm	a maximum sensitivity of 8.4 kPa ⁻¹ , a fast response time of <10 ms, high stability over >15,000 cycles and a low power consumption of <1 mW	[321]
Pressure	PDMS (PU)	R-GO/PU (AgNWs)/PEDOT:PSS/PUD	strain of 70% rolling, twisting, bending, and stretching	sensitivity of \approx 1.34% per °C, maintained its response after 10, 000 stretching cycles at the strain of 30%	[324]

^{a)} Referring to the spectral responsivity (R), detectivity (D^*), gain (G) and Response time (τ), limit of detection (LOD); ^{b)} referring to OECTs.

Author Bio

Haifeng Ling received his Ph.D. degree from the Institute of Advanced Materials (IAM), Nanjing University of Posts and Telecommunications in 2017, under the supervision of Prof. Wei Huang. He is currently working as a postdoctoral fellow in Prof. Feng Yan's group at The Hong Kong Polytechnic University. His research interests focus on organic flexible electronic devices including memories and sensors.



Shenghua Liu received his B.S. and M.S. degrees from University of Electronic Science and Technology of China in 2009 and 2012, respectively. Then he got his Ph.D. degree in the Hong Kong Polytechnic University in 2017. Currently, he is a postdoctoral fellow in the Department of Applied Physics at the Hong Kong Polytechnic University. Now, his research focuses on the fabrication and characterization of high efficient organic solar cells and flexible organic photovoltaics.



Feng Yan has research interests in thin film transistors, solar cells, 2D materials, organic electronics, biosensors and smart materials. He received his Ph.D degree in physics from

Nanjing University in China. Then he joined the Engineering Department of Cambridge University in Feb 2001 as a Research Associate and joined National Physical Laboratory in UK in April 2006 as a Higher Research Scientist. He became an Assistant Professor at the Department of Applied Physics of the Hong Kong Polytechnic University in September 2006 and was promoted to Professor in 2016.

The critical issues including material choice, device design, mechanical flexibility, strain effects and processing techniques and specific applications of flexible organic electronic devices are addressed in details. The performances of various flexible devices, like OFET, OLED and OPVs, are summarized and compared. Challenges and future development of this emerging field are presented in the end.

Keyword: Organic Electronics, Flexible, OLEDs, OPVs, OTFTs

*Haifeng Ling, Shenghua Liu, Zijian Zheng and Feng Yan**

Organic Flexible Electronics

ToC figure

